



Calhoun: The NPS Institutional Archive
DSpace Repository

Theses and Dissertations

1. Thesis and Dissertation Collection, all items

1993-12

X-ray pulse considerations and electron flow in high voltage vacuum diodes

Callahan, Michael O.

Monterey, California. Naval Postgraduate School

<http://hdl.handle.net/10945/39666>

Downloaded from NPS Archive: Calhoun



Calhoun is a project of the Dudley Knox Library at NPS, furthering the precepts and goals of open government and government transparency. All information contained herein has been approved for release by the NPS Public Affairs Officer.

Dudley Knox Library / Naval Postgraduate School
411 Dyer Road / 1 University Circle
Monterey, California USA 93943

<http://www.nps.edu/library>

AD-A277 301

2



NAVAL POSTGRADUATE SCHOOL
Monterey, California



DTIC
ELECTE
MAR 28 1994
S E D

THESIS

X-RAY PULSE CONSIDERATIONS AND ELECTRON FLOW
IN HIGH VOLTAGE DIODES
by
Michael O. Callahan
December, 1993
Thesis Advisor: Fred R. Schwirzke
Thesis Co-advisor: X. K. Maruyama

Approved for public release; distribution is unlimited.

94-08978



DTIC QUALITY INSURED

94 8 25 1994

REPORT DOCUMENTATION PAGE

Form Approved OMB No. 0704

Public reporting burden for this collection of information is estimated to average 1 hour per response, including the time for reviewing instruction, searching existing data sources, gathering and maintaining the data needed, and completing and reviewing the collection of information. Send comments regarding this burden estimate or any other aspect of this collection of information, including suggestions for reducing this burden, to Washington Headquarters Services, Directorate for Information Operations and Reports, 1215 Jefferson Davis Highway, Suite 1204, Arlington, VA 22202-4302, and to the Office of Management and Budget, Paperwork Reduction Project (0704-0188) Washington DC 20503.

1. AGENCY USE ONLY <i>(Leave blank)</i>	2. REPORT DATE 9 December 1993	3. REPORT TYPE AND DATES COVERED Master's Thesis
---	-----------------------------------	---

4. TITLE: X-RAY PULSE CONSIDERATIONS AND ELECTRON FLOW IN HIGH VOLTAGE VACUUM DIODES	5. FUNDING NUMBERS
--	--------------------

6. AUTHOR(S) CPT Michael O. Callahan	
--------------------------------------	--

7. PERFORMING ORGANIZATION NAME(S) AND ADDRESS(ES) Naval Postgraduate School Monterey CA 93943-5000	8. PERFORMING ORGANIZATION REPORT NUMBER
---	--

9. SPONSORING/MONITORING AGENCY NAME(S) AND ADDRESS(ES)	10. SPONSORING/MONITORING AGENCY REPORT NUMBER
---	--

11. SUPPLEMENTARY NOTES The views expressed in this thesis are those of the author and do not reflect the official policy or position of the Department of Defense or the U.S. Government.

12a. DISTRIBUTION/AVAILABILITY STATEMENT Approved for public release; distribution is unlimited.	12b. DISTRIBUTION CODE A
---	-----------------------------

13. ABSTRACT *(maximum 200 words)*

Electrical breakdown in high voltage diodes has been studied since the 1920s, yet it is still not well understood. This study characterizes the electron flow during breakdown in a high voltage vacuum diode. This was accomplished by measuring the x-rays produced when electrons strike the anode of the diode. Current measurements taken during the experiment include both the displacement and conduction electron current, so the x-ray signal is the best measure of the conduction current. Knowledge of the electron flow is important in determining the mechanism of breakdown.

The currently accepted explosive electron emission (EEE) model for electrical breakdown can not properly account for the energy required to form cathode spots. Schwirzke proposed a new model that involves an ionization process and a subsequent unipolar arc that accounts for the energy to form the spots. Electron flow for the two models is very different. The EEE model requires a large current density for several nanoseconds before plasma formation, whereas the new model predicts a large current density that develops simultaneously with the plasma formation. The results of this experiment support the predictions of the new model.

14. SUBJECT TERMS current density; cathode spot; vacuum diode; space charge; unipolar arc; x-ray	15. NUMBER OF PAGES 78
--	------------------------

	16. PRICE CODE
--	----------------

17. SECURITY CLASSIFICATION OF REPORT Unclassified	18. SECURITY CLASSIFICATION OF THIS PAGE Unclassified	19. SECURITY CLASSIFICATION OF ABSTRACT Unclassified	20. LIMITATION OF ABSTRACT UL
---	--	---	----------------------------------

NSN 7540-01-280-5500

Standard Form 298 (Rev. 2-89)

Prescribed by ANSI Std. Z39-18

Approved for public release; distribution is unlimited.

X-ray Pulse Considerations and Electron Flow in High Voltage Vacuum Diodes

by

Michael O. Callahan
Captain, United States Army
B.A., University of Rochester, 1985


Submitted in partial fulfillment
of the requirements for the degree of

MASTER OF SCIENCE IN PHYSICS

from the

NAVAL POSTGRADUATE SCHOOL
December 1993


Author:


Michael O. Callahan

Approved by:


Fred R. Schwirzke, Thesis Advisor


Xavier K. Maruyama, Co-advisor


William B. Colson, Chairman,
Department of Physics

ABSTRACT

Electrical breakdown in high voltage diodes has been studied since the 1920s, yet it is still not well understood. This study characterizes the electron flow during breakdown in a high voltage vacuum diode. This was accomplished by measuring the x-rays produced when electrons strike the anode of the diode. Current measurements taken during the experiment include both the displacement and conduction electron current, so the x-ray signal is the best measure of the conduction current. Knowledge of the electron flow is important in determining the mechanism of breakdown.

The currently accepted explosive electron emission (EEE) model for electrical breakdown can not properly account for the energy required to form cathode spots. Schwirzke proposed a new model that involves an ionization process and a subsequent unipolar arc that accounts for the energy to form the spots. Electron flow for the two models is very different. The EEE model requires a large current density for several nanoseconds before plasma formation, whereas the new model predicts a large current density that develops simultaneously with the plasma formation. The results of this experiment support the predictions of the new model.

Accession For	
NTIS	CRA&I <input checked="" type="checkbox"/>
DTIC	TAB <input type="checkbox"/>
Unannounced <input type="checkbox"/>	
Justification	
By	
Distribution /	
Availability Codes	
Dist	Avail and/or Special
A-1	

--

TABLE OF CONTENTS

I.	INTRODUCTION	1
II.	BACKGROUND	3
	A. REVIEW OF DIODE PHYSICS	3
	B. ELECTRIC FIELD ENHANCEMENT - THE β FACTOR	5
	C. EXPLOSIVE ELECTRON EMISSION MODEL	6
III.	DNI MODEL	8
	A. BASIS FOR THE DNI MODEL	8
	B. QUALITATIVE DESCRIPTION OF DNI MODEL	9
	1. Initial Conditions and Neutral Desorption	9
	2. Onset of Ionization	9
	3. Field Emission, Plasma Formation, and the X-ray Pulse	10
	4. Predictions Based on the DNI Model	12
IV.	EXPERIMENT	14
	A. OVERVIEW	14
	B. Experimental Setup	15
	1. Equipment and Laboratory Layout	15
	2. Signal Processing Configuration	18
	3. Optical Setup	18
	4. X-ray Setup	20

C.	PROCEDURES	22
	1. Voltages	22
	2. Timing	23
	3. Optical Delay Corrections	25
	4. X-ray Delay Corrections	25
	5. Data Acquisition	25
D.	EXPERIMENTAL CONCERNS	26
	1. Electromagnetic Noise	26
	2. Stray X-rays	27
V.	EXPERIMENTAL RESULTS	28
A.	EXAMPLE WAVEFORMS	28
	1. 55kV Examples	29
	2. 75kV Examples	32
	3. 100kV Examples	36
B.	Superimposed Digitized Waveforms	40
C.	Average Onset Times	47
VI	ANALYSIS	48
A.	COMPARISON OF ACTUAL AND PREDICTED PLASMA ONSET	48
B.	X-RAY ONSET	50
	1. Overview	50
	2. Displacement Current	51
	3. Field Emission and Enhanced Field Emission .	53
C.	LIMITATIONS OF INTERPRETATION	54
	1. Child-Langmuir Current Limitation	54

2. X-ray Detector Efficiency	54
3. Relativistic Considerations	55
4. Electromagnetic Noise	55
VII CONCLUSION AND RECOMMENDATIONS	57
A. CONCLUSION	57
B. RECOMMENDATIONS	58
APPENDIX A: DATA	60
APPENDIX B: ERROR ANALYSIS	64
A. TIME MEASUREMENTS	64
B. VOLTAGE MEASUREMENTS	65
LIST OF REFERENCES	67
INITIAL DISTRIBUTION LIST	69

ACKNOWLEDGEMENTS

This work was a great learning experience, and I would like to express my appreciation to some of the people who helped along the way. My thanks to Professor Schwirzke for his patience through the many questions, and for helping me make sense of plasma physics. Thanks to Professor X.K. Maruyama for his experimental insights, and for letting me use his lab. Thanks to Don and Harold for answering many dumb questions, letting us use their stuff, and certifying us in flash x-ray operations. Thanks also to Chas Wright, [Ref. 10] my partner, for putting up with "bike riding time". Finally, thanks to my wife Alison and my daughters Taryn and Gillian for all their understanding and support.

I. INTRODUCTION

The mechanism of electrical breakdown on electrodes is important in many fields, yet it is still not well understood. It is most important in high power switching, particle beam generation, and pulsed power technology. Better understanding of the breakdown process could lead to improved component designs for these applications that provide longer component lifetimes and more energy efficient systems.

The phenomena of breakdown have been studied since the 1920's yet numerous competing theories still exist. All theories agree that there is cathode spot formation [Refs. 1,2], and that it is a plasma mechanism, but the similarities end there. A cathode spot is a crater on a cathode surface that is formed by a plasma mechanism when a high voltage (strong electric field) acts on that surface. The current most widely accepted model for cathode spot formation is the explosive electron emission (EEE) model [Ref. 2]. This model proposes that a high electron current passing through a microprotrusion or whisker on the cathode surface causes explosion of the whisker and formation of the cathode spot. There is some doubt as to whether this mechanism can provide enough energy to explode a whisker [Refs. 3,4]. A new model, proposed by Schwirzke [Ref. 5], proposes a more complex process involving ionization, that can provide the energy required to form the cathode spot.

This work builds upon previous NPS work and could be the basis for future work in this area. The experiment described here was done using the high voltage vacuum diode of the Naval Postgraduate School Flash X-ray machine. It examines the time scale of the x-ray pulse that occurs during cathode spot formation and relates it to the electron flow in the diode. This x-ray pulse will be compared to the voltage, current, and plasma (light) onset times to determine how the plasma formation evolves. The x-ray signal is a direct indicator of electron flow across the diode gap. The current signal measures both displacement and conduction current, so the x-ray signal provides important information, especially early in the voltage buildup when the displacement current could be large. Using the x-ray signal as a relative measure of the conduction current, we can determine whether a high current causes plasma formation, or is the result of enhanced electron emission after plasma formation.

This study is organized to provide an overall view of the breakdown process, then to describe and analyze the x-ray pulse timing. It starts with basic diode physics and background in the next chapter. Chapter III covers the Schwirzke model, and Chapters IV, V, and VI cover the experiment, results and analysis respectively. The conclusion summarizes the analysis and will show that the measured x-ray pulse can be used to support the new model.

II. BACKGROUND

A. REVIEW OF DIODE PHYSICS

A planar high voltage diode consists of two conducting plates separated by a distance, d , that is small compared to their surface dimensions. The gap between the plates is evacuated, in this case to a high vacuum (10^{-5} - 10^{-6} Torr). When a high enough voltage is applied across the gap, breakdown occurs, a current flows, and the gap is eventually filled with a conducting plasma, this latter stage being termed diode closure.

The electric field (E) in a planar diode before current begins to flow in the gap is;

$$E = \frac{\Phi_0}{d} \quad (2.1)$$

where Φ_0 is the applied voltage potential. When current begins to flow, the changing charge distribution affects the electric field. This is known as a space charge effect (Fig. 2.1). For high voltage diodes like the one used for this experiment, the potential minimum is negligible compared to the high applied potential and the minimum (Fig. 2.1, IV) is practically coincident with the cathode surface. In this case, the electric field vanishes at the cathode surface and

the emitted electrons have zero initial velocity. This makes the electron flow space charge limited. [Ref. 6]

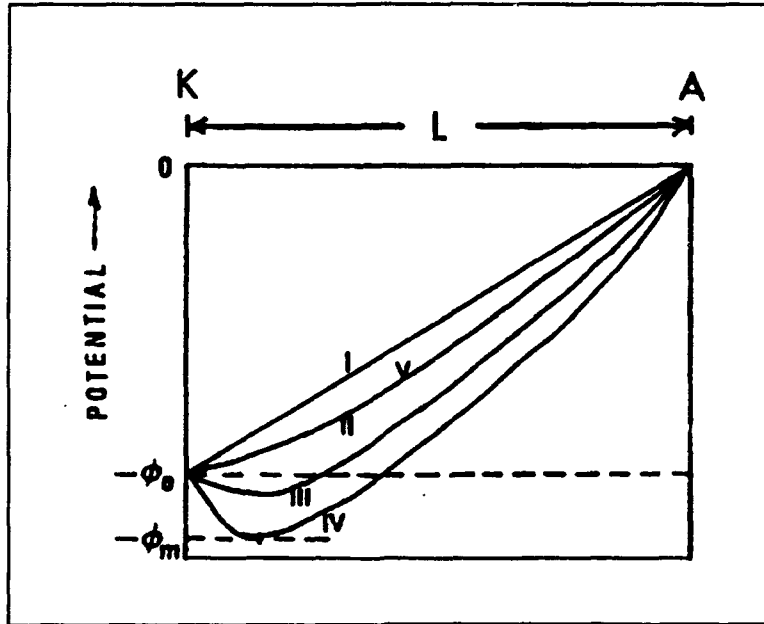


Figure 2.1 Electrostatic Potential in a Diode Including Electron Space Charge. I through IV are sequential in time.

When the macroscopic field in a diode reaches 10^6 - 10^7 V/m, electrons are emitted from the cathode through a quantum mechanical phenomenon called field emission. Field emission current densities (j_{fe}) are governed by the Fowler Nordheim (FN) equation:

$$j_{fe} = c_1 \beta^2 E^2 \exp\left(-\frac{c_2}{\beta E}\right) \quad (2.2)$$

where β is the electric field enhancement factor, and c_1 , and c_2 are constants. For large values of E , j_{fe} is proportional to $\beta^2 E^2$. The FN equation seems to indicate that the electron

current will continue to increase with the electric field. In reality, the current is limited by the previously indicated space charge consideration. Using a nonrelativistic treatment, the space charge limited current density (j_{cl}) is given by the Child-Langmuir expression:

$$j_{cl} = \frac{4}{9} \epsilon_0 \left(2 \frac{e}{m} \right)^{1/2} \frac{\Phi_0^{3/2}}{d^2} \quad (2.3)$$

where ϵ_0 is the permittivity of free space, e is the magnitude of the charge carriers, m is the mass of the charge carriers, Φ_0 is the diode potential and d is the distance from the zero potential to the potential Φ_0 [Ref. 6]. The Child Langmuir expression represents an upper bound to the space charge limited current that can flow in the diode. The nonrelativistic treatment used in this case is based on the previous work of Hallal [Ref. 3]. Hallal's work also provided the basis for ignoring the effects of parapotential flow [Ref. 6]. Although some relativistic effects may be important for electron flow in the diode, these effects do not alter the conclusions of this experiment.

B. ELECTRIC FIELD ENHANCEMENT - THE β FACTOR

Depending on the specified use of a diode, the electrode surfaces can range from polished and clean to rough and dirty. Polished and clean electrodes are known to have microscopic

projections (μm size) called whiskers with densities up to 10^4 whisker/ cm^2 [Ref. 6]. Because the electric field flux is greater at the whisker tip, these whiskers can lead to significant electric field enhancement (Fig. 2.2). The field enhancement factor β is important in determining where and when electron field emission starts. Values of this factor range up to several hundred [Ref. 6].

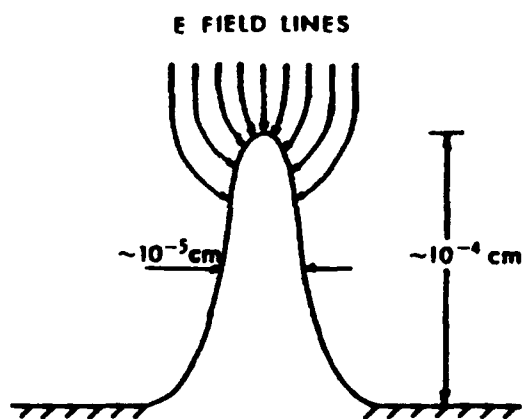


Figure 2.2 Electric Field Enhancement at a Whisker Surface. [Ref. 6]

C. EXPLOSIVE ELECTRON EMISSION MODEL

The current most widely accepted model for breakdown in high voltage diodes is the Explosive Electron Emission (EEE) model proposed by Mesyats [Ref. 2]. This model proposes that the resistive heating of field emission currents causes

explosion of whiskers into a dense plasma and hence, the formation of cathode spots. The rapidly expanding plasma then covers the cathode surface leading to even higher current. The plasma expansion into the gap continues until diode closure when the voltage is effectively short circuited.

The initial plasma formation is known to occur within nanoseconds ($\sim 10\text{ns}$) [Ref. 2,3] for short ($\sim 10\text{ns}$) pulse risetimes. Estimates of current densities required to explode a whisker in the EEE model are $j_{ie} = 10^{11}-10^{13}\text{A/m}^2$ [Refs. 2,3,6]. For a diode like the one used in this experiment, with $\Phi_0 = 1\text{MV}$ and $d=2.54\text{cm}$, Equation 2.3 gives $j_{cl} = 3.6 \times 10^6 \text{ A/m}^2$. If the Child-Langmuir current density (j_{cl}) represents an upper bound, then, $j_{ie} = j_{cl} \ll 10^{11}\text{A/m}^2$, and explosion of the whisker by this method is not possible.

The EEE Model does not properly describe the "explosive" formation of cathode spots. What, then, is the mechanism for breakdown at the cathode? To answer this, Schwirzke and Hallal presented a new model that takes into account ionization of neutrals and their return kinetic energy at the cathode [Ref. 3]. For future reference, this model will be called the desorbed neutral ionization (DNI) or Schwirzke model.

III. DNI MODEL

A. BASIS FOR THE DNI MODEL

The new model for cathode spot formation must include a mechanism that delivers orders of magnitude more energy on the nanosecond time scale. If, by some mechanism, an ion space charge could be established it would increase the field emission current, but it could not provide the increased orders of magnitude of current required to explode the whisker. The DNI model includes not only the build up of ion space charge, but also as source of energy the kinetic energy of ions accelerated to the cathode, and the subsequent formation of an unipolar arc [Ref. 7]. The kinetic energy is efficiently transferred to the surface layer of the cathode and provides energy for desorbing neutrals that are ionized and further enhance the electric field leading to the unipolar arc and formation of cathode spots. Reference 3 covers the details of the kinetic energy transfer. This work will focus on the temporal characteristics of the initial field emission, ionization and plasma formation with emphasis on the x-ray pulse that occurs during the process.

B. QUALITATIVE DESCRIPTION OF DNI MODEL

1. Initial Conditions and Neutral Desorption

Even the cleanest electrodes are known to have at least some contamination on their surfaces. Adsorbates like CO₂, O₂, and acetone (used for cleaning most vacuum surfaces) molecules are weakly bound to the surface by Van der Waals attractions $\approx 0.25\text{eV}$ molecule [Ref. 5]. If these adsorbates were released from the cathode, they could be ionized by the field emission current. The ions then provide the energy required to explode a whisker. A suddenly released single layer of 2×10^{19} molecules/m² expands into a vacuum with speed, $v \approx 470\text{m/s}$ [Ref. 8], providing near atmospheric densities in front of the cathode within nanoseconds [Ref 5]. The mechanism of release of these adsorbates is thought to be the onset of the electric field, impact of ions, electron emission, and possibly the displacement current. The role of the displacement current will be discussed further in the analysis of results.

2. Onset of Ionization

The dense neutral cloud ($n_0 = 10^{25}/\text{m}^3$) expanding in front of the cathode can provide a ready source for ions. As a voltage is applied across the diode and the macroscopic electric field reaches $10^6 - 10^7$ V/m, field emission of electrons begins in places with enhancement factors, $\beta \geq 100$. These field emission electrons provide the ionization. The neutrals have a maximum cross section for ionization near 100V (using oxygen

as a typical case) [Ref. 9]. As the diode voltage rises, the 100V equipotential surface (EPS) moves closer to the cathode as the neutrals expand outward. Figure 3.1 shows the progress of the neutrals and the 100V potential for three typical maximum diode voltages with approximated linear risetimes of about 20ns. Predicted onset of ionization is in the area near where the two curves meet, there being a significant chance of ionization. The delay of ionization, or plasma formation can be measured by detecting the light signal at the cathode.

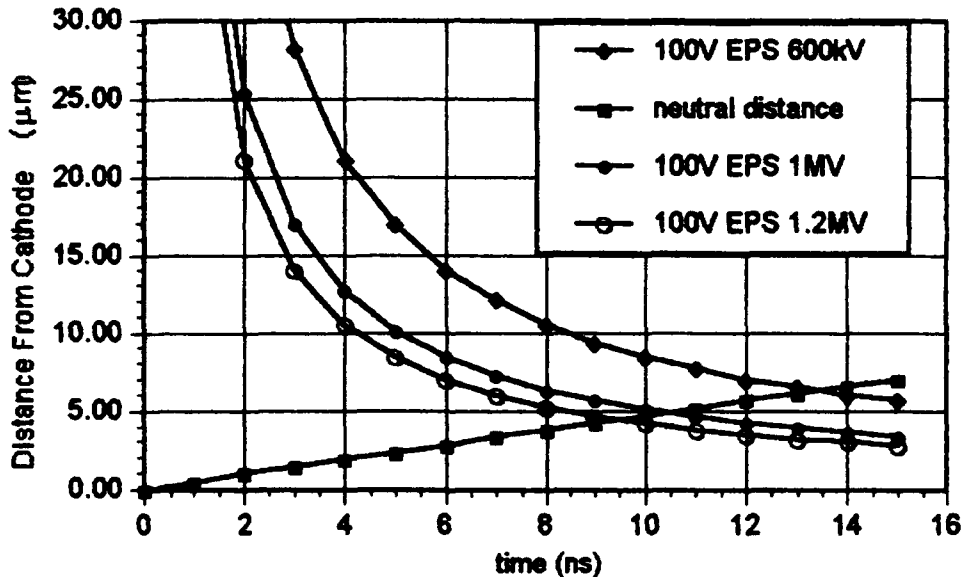


Figure 3.1 100V EPS and Neutral Distance From the Cathode vs Time From Voltage Onset. Assumed pulse rise time is 20ns.

3. Field Emission, Plasma Formation, and the X-ray Pulse

When an increasing voltage is applied and field emission of electrons begins at $E \approx 10^7$ V/m, from individual spots with large enhancement factors β , the emitted electrons are of relatively low energy ($E \approx 25$ keV). When these electrons

arrive at the anode, they produce x-rays through bremsstrahlung and absorption edge processes. As the voltage rises, and ionization begins at the cathode, the electric field in front of the emitting spot on the cathode is further enhanced by the ion space charge, and the field emission current density increases by the FN equation (Eq 2.3). The increasing current further increases ionization, causing an even more dense layer of positive space charge to develop above the emission site. As a dense plasma forms, it shields the cathode from the applied electric field. The increasing current density and ion bombardment heat the cathode and finally cause thermionic electron emission, which provides a source of electrons for an unipolar arc (Fig. 3.2) [Ref. 5].

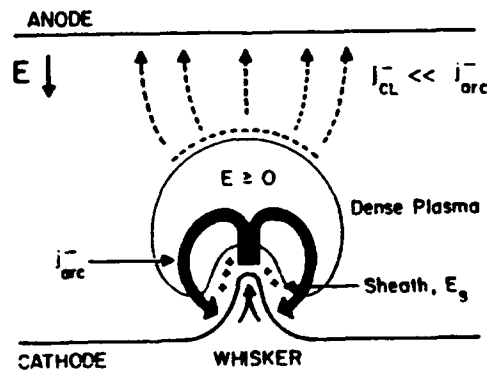


Figure 3.2 Unipolar Arc Schematic. [Ref. 5]

The plasma formation as indicated by the cathode light signal has been measured to develop with a risetime on the order of a few nanoseconds. The cathode plasma now acts as a source of electrons that respond to the externally applied potential. A dramatic increase in x-rays should coincide with the plasma formation due to the availability of electrons from the dense cathode plasma.

Throughout this process, electrons that reach the anode produce a broad spectrum of x-rays that varies with the electron energy. The onset of this x-ray pulse and its relative magnitude will be studied to provide further insight into the plasma formation.

4. Predictions Based on the DNI Model

The most important temporal parameters in the DNI model are the transit time of the neutrals to the ionization region a few μm from the cathode surface and the position of the 100V potential based on the voltage risetime. When the 100V potential and neutral density have a significant overlap (Fig. 3.3) ionization begins and the process develops rapidly from there. If the EEE model correctly describes cathode spot formation, the high j_e would produce a significant x-ray signal for several nanoseconds prior to plasma formation. The DNI model predicts that the initial x-ray signal from the field emission will be small, with a rapid build up near the onset of plasma formation due to the enhanced field emission brought about by ionization. The one underlying assumption

here is that the x-rays are a direct measure of electrons flowing across the diode gap. In this experiment, plasma formation will be measured by the onset of light production in the diode, and the x-ray signal will then be compared to the voltage, current, and plasma onset times.

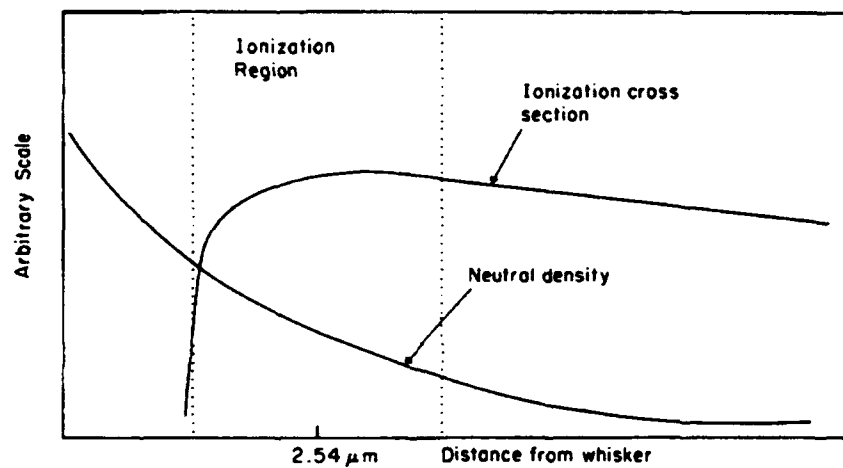


Figure 3.3 Schematic of a Typical Ionization Cross Section and Neutral Density Distribution Shortly After the Voltage is Applied. [Ref. 3]

IV. EXPERIMENT

A. OVERVIEW

This experiment is designed to determine the time scale of five important plasma formation parameters. The parameters to be measured were: diode voltage, diode current, anode and cathode light pulses, and the breakdown x-ray signal. The setup was used for two different experiments; one studying the temporal response of visible light produced at the anode and cathode [Ref. 10], and this one studying the correlation between the cathode light (plasma) production and the x-ray pulse that occurs during electrical breakdown when electrons emitted from cathode plasma reach the anode. Both experiments compare the onset of plasma formation to the voltage pulse onset and relate these to the model in Chapter III.

The need to determine all five parameters on the same firing of the flash x-ray (FXR) machine made the setup complex. To simplify the description, the experimental setup is divided into electrical, optical and x-ray component set ups.

B. Experimental Setup

1. Equipment and Laboratory Layout

This experiment was performed at the Naval Postgraduate School (NPS) FXR facility using a Physics International Company Pulserad 112A flash x-ray machine. A layout of the FXR facility is shown in Fig 4.1 [Ref. 11]. The pulserad 112A accelerates electrons across a high vacuum (10^{-5} - 10^{-6} Torr) diode. The current pulse at full width half maximum (FWHM) is 20-25 nanoseconds. The diode potential can be varied from 600kV to 1.6MV. The diode gap for the pulserad is 2.5 cm, and the cathode is stainless steel. The anode used was 15 mil tantalum for x-ray measurement. Later, a solid stainless steel anode was used to further examine the anode and cathode light pulses and damage mechanisms [Ref 10]. For a complete description of the Pulserad 112A see Reference 12.

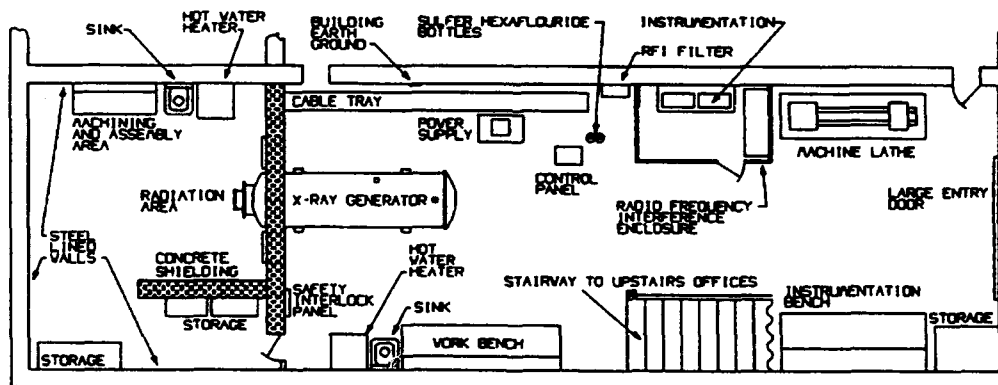


Figure 4.1 Layout of the FXR Facility. [Ref. 11]

The diode voltage and current were measured by installed monitors supplied with the Pulserad. The signals from these monitors were measured by Tektronix 7104 1GHz oscilloscopes and Tektronix Digital Camera Systems (DCS). The voltage signal required 46dB attenuation, and the current 20dB attenuation to be viewed on the oscilloscopes. The absolute magnitudes of these signals had significance in this experiment so they must be calculated based on the oscilloscope trace. Actual diode voltage (V) is determined by;

$$V_{ac} [kV] = 320 V_{scope} \quad (4.1)$$

and diode current (I) is determined using,

$$I_{ac} [kA] = 7.31 V_{scope} \quad (4.2)$$

[Ref. 12].

Fast risetime (400ps) photodetectors with optical fiber input were used to measure the plasma light signals, and a foil shielded photodetector (150ps risetime) was used to measure the x-ray pulse. The anode, cathode, and x-ray signals were measured using two Tektronix DSA 602A digital signal analyzers (DSA) with 1 GHz bandwidth. Each DSA is two channel capable at 1GHz so the anode and cathode signals were recorded on the same DSA. Table 4.1 shows the detection and measurement equipment used and its important operating characteristics.

Table 4.1 DETECTION AND MEASURING EQUIPMENT USED FOR EXPERIMENT

Equipment	Purpose	Manufacturer/ Model	Characteristics	Ref.
Photo Detector	Detect Plasma Light Pulse	NewFocus/ Model 1601	1GHz BW ±15V Bias 400ps Risetime	13
X-ray Detector	Detect X-ray pulse	Lasermetrics/ Series 3117 Type I	PIN Silicon 150ps Risetime 100V Reverse Bias	14
Voltage Divider	Detect/Send Voltage Pulse	Physics International/ PIM-197A25	±5% Accuracy 1.6kV/V Sensitivity	12
Fluxmeter	Current Detector	Physics International/ PIM-199B	±5% Accuracy .872kV/T Sensitivity	12
Oscilloscope (2)	Acquires Voltage and Current Waveforms	Tektronix/ 7104 w/7B92A Time Base	1GHz BW ±3% Timebase Accuracy	15
Digitizing Camera System	Measures and Records Oscilloscope Waveforms	Tektronix/ DCS 01	512 Pixels/Sweep Use w/7104 Scopes	16
Digitizing Signal Analyzer	Acquires, Measures, and Records Light and X-ray Waveforms	Tektronix/ 602A w/ 11A34 Plug In	1GHz BW (2 Channel) Disk Drive Storage Spreadsheet Files ±0.03% Timebase Accuracy	17

2. Signal Processing Configuration

The signal processing arrangement allowed simplified data acquisition of five simultaneous waveforms. A Stanford Research Digital Delay Generator, DG-535, was used to synchronize the wave forms. Figure 4.2 shows a schematic drawing of the signal processing setup.

To synchronize the time scales of the measured waveforms, the oscilloscopes and DSAs had to be externally triggered before arrival of their signals. The Marx Bank voltage signal was used as the base trigger because it occurs significantly (50-150ns) before the diode voltage, diode current, and plasma signals. The Marx signal then triggers the delay generator which in turn tells each oscilloscope or DSA when to "look" for a signal. The delays on the DG-535 are set based on a timing procedure covered in the "timing" section. The final result is that the timing information from all waveforms of a single firing is directly comparable.

3. Optical Setup

Two New Focus Model 1601 photodetectors were used to convert the light signal produced at the anode and cathode into an electrical signal which could be recorded by the DSA. The detectors were housed in a 1.25cm thick aluminum barrel to reduce electromagnetic noise. They were biased to $\pm 15V$ and their outputs were connected to heavily shielded, high frequency capable, coaxial cables. Two fiber optic bundles, 0.125 inches in diameter and 1.85m long had one end coupled to

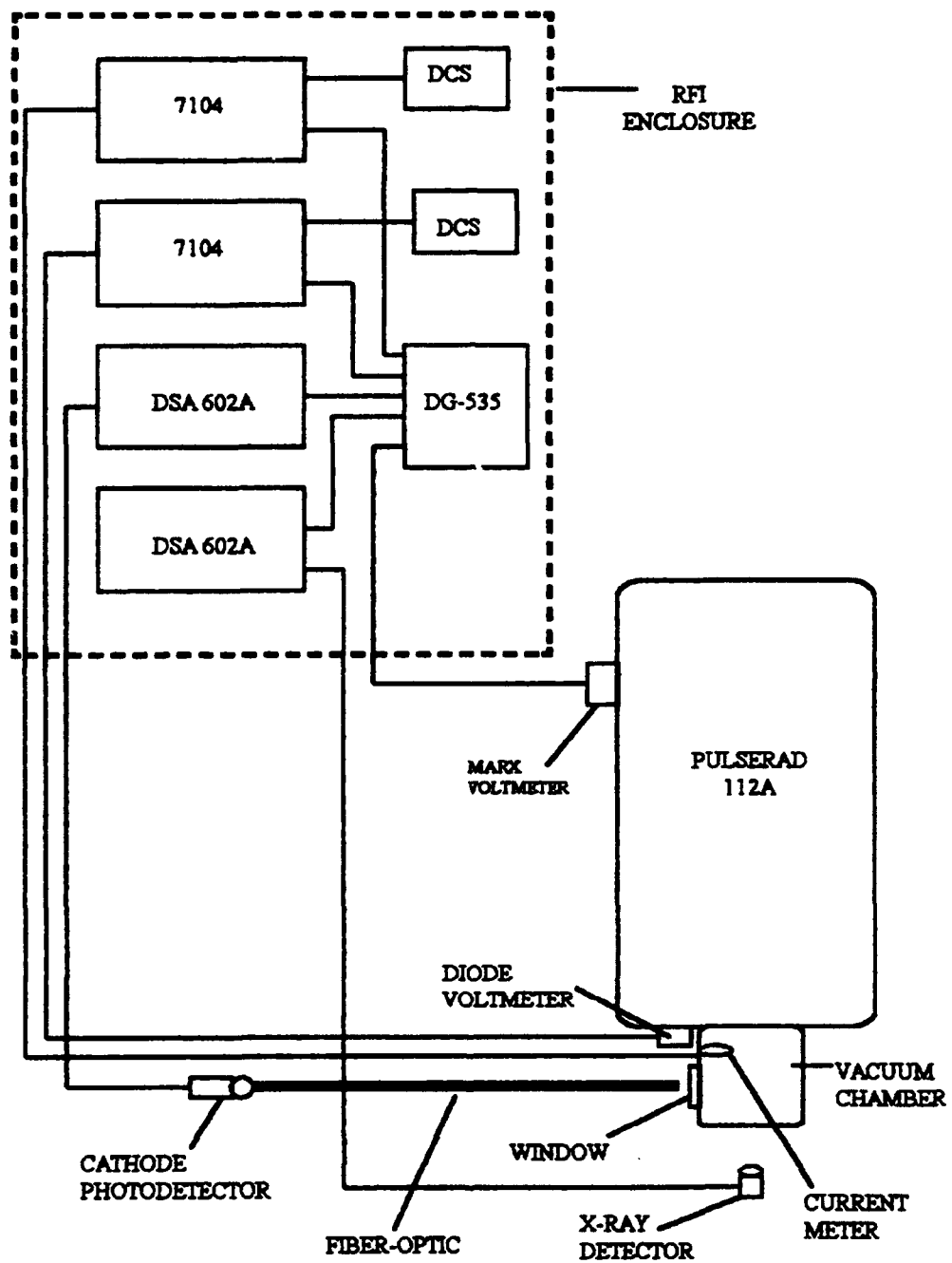


Figure 4.2 Signal Processing Schematic.

the photodetector's optically sensitive area. The other end was fed through drilled holes of a lead brick. The lead bricks were needed to prevent x-rays from registering on the light detectors. This is discussed in greater detail in section D of this chapter. The protruding ends of the fiber optic cables were then separated by a 0.7cm thick aluminum plate which was placed flush against the vacuum chamber window and centered on the middle of the diode gap. This plate served to block light produced on the cathode surface from entering the fiber optic cable positioned to receive light from the anode and vice versa. Only the cathode light signal was recorded for this experiment.

4. X-ray Setup

X-ray signal detection and measurement was the one procedure that had not been done in previous plasma formation experiments at the NPS FXR facility. Finding the right detection equipment required consultation with some detector "experts", and considerable trial and error. Scintillation type detectors were considered, but ruled out due to difficulties in eliminating extraneous signals. Consultations with Mr. George Berzins at Los Alamos National Laboratory, and Mr. Ray Muller at Hamamatsu Corp. indicated that a biased PIN photodiode could be used if we were interested only in the time resolution, and not dose or frequency information. After trying a few detectors, the Lasermetrics Series 3117 Type I

photodiode with its switchable power supply was selected as the most cost effective solution.

Previous experiments at the FXR by Galarowicz [Ref. 11] showed that placement of the detector along the axis of the FXR provided the maximum x-ray dose. The detector was shielded with household aluminum foil to keep out visible light, and reduce electromagnetic noise. Final photodiode positioning was then determined by taking a series of shots at different distances and voltages to get a high (10:1) signal to noise ratio without saturating the detector. In the operating range of the detector, the signal amplitude was found to be proportional to the radiation dose received, so proper placement of the detector was a matter of checking the radiation dose. The Marx voltages selected for the experiment; 55kV, 75kV and 100kV required the detector to be placed at 13cm, 28cm, and 80cm respectively from the end plate of the FXR. Doses at 75kV and 100kV were also reduced by the use of a 1.25cm lead shield with a 1.25cm aperture along the axis of the diode. The detector was aligned with the diode axis using the marked geometric center of the FXR diode. Variations of a few millimeters off axis of the diode were inconsequential for this experiment. Figure 4.3 shows a side view of the X-ray detection setup at the diode end of the FXR. The cathode of the FXR is visible through the window of the vacuum chamber (left side of the photo). The x-ray detector

is in the center mounted on a steel rod. The detector power supply is below and to the right of the detector.



Figure 4.3 Side View of the X-ray Detection Setup.

C. PROCEDURES

1. Voltages

Three different FXR diode voltages were examined in this experiment. The diode voltage is the parameter that we use when observing plasma formation, but the FXR machine is set for firing by the Marx Bank charge. The diode voltage for each shot is a function of the Marx Bank charge and the diode impedance. The impedance changes slightly from shot to shot, and so does the diode voltage. For convenience, the shots are normally referred to by their Marx Bank charge. Marx Bank charges for this experiment were 55kV, 75kV, and 100kV, which correspond to diode voltages of 600kV, 1MV, and 1.2MV respectively.

2. Timing

Ensuring that all of the recorded waveforms were synchronized was a crucial part of the data collection effort. Our method of synchronization compensated for all time differences in the transmission line - oscilloscope system to include time base and response time characteristics of the oscilloscopes and the length and impedance differences of the transmission cables. To do this we used a Hewlett Packard pulse generator to send a 20ns pulse down the transmission cables of two of the measuring devices (eg. x-ray and light) simultaneously. We then compared the recorded onset times of the pulse and adjusted the delay generator so that they occurred at the same time (within 0.3ns). Because we could synchronize only two transmission line - oscilloscope systems at one time, we established one system as the base system and synchronized the other three with respect to that base. In this way they were all synchronized to each other. For our purposes we used the x-ray line - digitizer system as the base because it has the shortest cable length, hence its delay was defined as zero and synchronization could be accomplished by adding delays to the other systems. We performed our timing in the following manner:

In the Diode Room:

1. Attach two cables of the same length to a "T" connector and attach the "T" connector to the output BNC connector of the pulse generator.
2. Attach one end of a cable to the trigger output of the pulse generator and the other end to the unused "B" twisted coax cable.
3. Put the following settings on the pulse generator: Pulse width - 20ns, mode - manual trigger, attenuation - 5dB, trigger advance - 140ns, wave shape - square.
4. Attach one of the signal output cables to the x-ray detector cable, and attach the other output cables to the cable of the system you wish to synchronize (i.e. voltage, current or light detector cables). Note; you must remove the attenuators from the voltages and current cable first or the signal will be too small.

In the RF Protected Cage:

5. Remove the Marx charge line from the trigger input connector of the Delay generator and replace it with the "B" coax cable.
6. Ensure oscilloscope/waveform digitizers are set to 1V/div, 10ns/div and external trigger. Then put in the acquire mode.
7. Set all delays to zero on the delay generator.
8. Manually trigger the pulse generator and compare and record onset times of the acquired waveforms. Note; disregard waveforms with ambiguous onset times.
9. Adjust the delay generator corresponding to the system being synchronized to match the difference recorded in Step 8.
10. Trigger the pulse generator again and compare onset times. If the difference is less than 0.3ns, the two systems are synchronized. Change cable connections and repeat steps 8 and 9. If the difference in the onset times is greater than 0.3ns, adjust the delay generator half the difference and repeat steps 8, 9 and 10 until the difference is less than 0.3ns.

After completing these steps all cable - scope systems are accurately synchronized but you must add 25ns (55kV shots) and 125ns (75kV and 100kV shots) additional delay to all of the systems on the delay generator to ensure the waveforms appear within the screen when triggered by the Marx voltage signal.

In addition you must apply the following timing corrections to account for transit times of the light and x-rays.

3. Optical Delay Corrections

The light produced on the electrodes must travel 15cm to the vacuum chamber window and an additional 7.5cm beyond that to the end of the 1.83m long fiber optic cable which has an index of refraction of $n=1.62$. Using the relation $t=x/v$ for the two mediums yields a correction of $t=10.7\text{ns}$. This delay must be added to the delay generator for the light system.

4. X-ray Delay Corrections

X-rays produced on the anode must travel to the x-ray detector located a distance l behind the anode. The position l varied between 30cm and 1m depending on the magnitude of the voltage shot being measured. This resulted in x-ray delay corrections between 1 and 3 nanoseconds.

5. Data Acquisition

To obtain the desired waveforms, the Marx Bank capacitors must be charged in parallel and discharged in series across the diode gap. To ensure this is done properly, use the following checklist:

Data Acquisition:

1. Reconnect all cables and attenuators that were disconnected during the timing process.
2. Turn on and properly bias the photo and x-ray detectors.
3. Reset the voltage levels on the oscilloscopes/DSAs and put them in the acquire mode.
4. Set the pressures on the control switches in accordance with the pressure chart.
5. Charge the Marx Bank by turning on all power switches, turning the keys and depressing the charge buttons.

6. Once the Marx Bank is charged to the voltage you have preselected, the ready light will come on. Press the trigger button and the voltage will be released across the diode. All wave forms will appear on the oscilloscopes/DSAs.

For this experiment, one set of ten shots was done at each of the three different Marx Bank charge ; 55kV, 75kV, and 100kV. These Marx Bank charges translate roughly into diode voltages of 600kV, 1MV and 1.2MV respectively. Averages were done on the ten shots to determine onset times. Additionally one "blackout" shot was done for each voltage by shielding the x-ray and light detectors from their respective signals. This served to measure the noise generated in the photo and x-ray detectors. The x-ray detector was shielded with two 5cm thick lead bricks, and the light detectors were covered by opaque tape.

D. EXPERIMENTAL CONCERNS

1. Electromagnetic Noise

As with previous experiments at the NPS FXR, electromagnetic noise proved to be a troublesome problem to overcome. By using many of the techniques mentioned in previous work [Ref. 11], such as extensive use of aluminum foil for RF shielding and the placement of the photo detectors as far away from the vacuum chamber as possible the noise problem became manageable. Another successful improvement we made to the system configuration was to attenuate the relatively high voltage signals (diode and Marx voltages) at the source rather than at the oscilloscope. This reduced the

amount of noise pickup in the transmission lines of the photo and x-ray detectors. The aluminum barrel housing used for the photodetectors also helped reduce E&M noise though it was more effective in attenuating x-rays.

2. Stray X-rays

As discussed earlier X radiation can produce a large signal on silicon diode photodetectors designed to measure visible light. Even with the photodetectors more than 2m away from the vacuum chamber, x-rays produced a sizable signal ($\approx 5\text{mV}$) on the photodetectors. To block the x-rays from reaching the detectors, we stacked 5cm thick lead bricks in front of the detectors. Surprisingly, this only slightly alleviated our problem. Through trial and error we found it necessary to block the x-rays from irradiating the fiber optic cables which have a metallic casing. We did this by running the cables through two small holes drilled through a 5cm thick lead brick. Though we do not understand why this worked we are convinced of its effectiveness.

V. EXPERIMENTAL RESULTS

There are many problems working in the high noise FXR environment. It seemed that every data run had some type of complication. As my experience with the equipment grew, so did my confidence in the data I recorded. Most of the initial trial work was done with a 75kV Marx charge, where the noise factors were reasonable, and signal to noise was quite good. In the 55kV data run, there were some problems with signal to noise, but the timing seemed good. The 100kV data runs were subject to high EM noise, and there seemed to be a problem with current timing. I will highlight some of the problem areas with the following examples, but will defer a detailed discussion to Chapter VI.

A. EXAMPLE WAVEFORMS

The following are examples of the data signals. There is one set from each of the three Marx bank charges (55, 75, and 100kV). All of the signals for a given Marx charge are synchronized as they are from the same shot or run. Time comparisons between different shots must be done based on times from voltage onset. Comparison of actual times (measured by DCS or DSA) for different shots is meaningless since the timing of the Marx firing changes slightly from shot to shot. Times for all data runs are in Appendix A.

Additionally, the blackout signals for both x-ray and cathode detectors are shown for each Marx voltage. To compare the blackout signal to the data signal, the voltage onset times must be compared. The actual diode voltage and current values can be determined using Eqs. 4.1 and 4.2 respectively. In a following section, I will digitize and scale the four waveforms from each run for direct temporal comparison.

1. 55kV Examples

Figures 5.1 through 5.4 show the diode voltage, diode current, x-ray, and cathode light signals for a typical 55kV shot. Figures 5.1 and 5.2 show that the current waveform follows the voltage, as it does in all cases. Figures 5.5 and 5.6 are the blackout signals for x-ray and light respectively. although the noise in Fig. 5.5 is substantial, it occurs well after an x-ray signal would be detected.

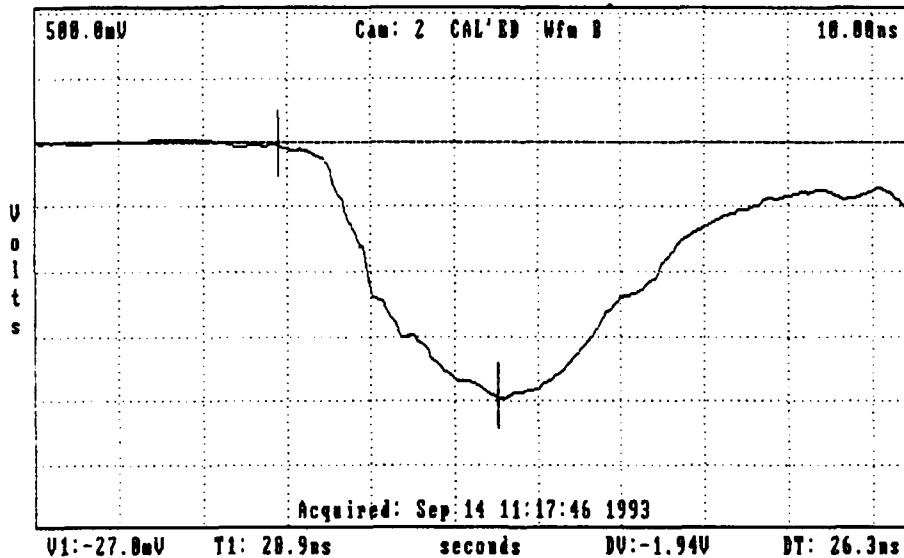


Figure 5.1 Diode Voltage 55kV.

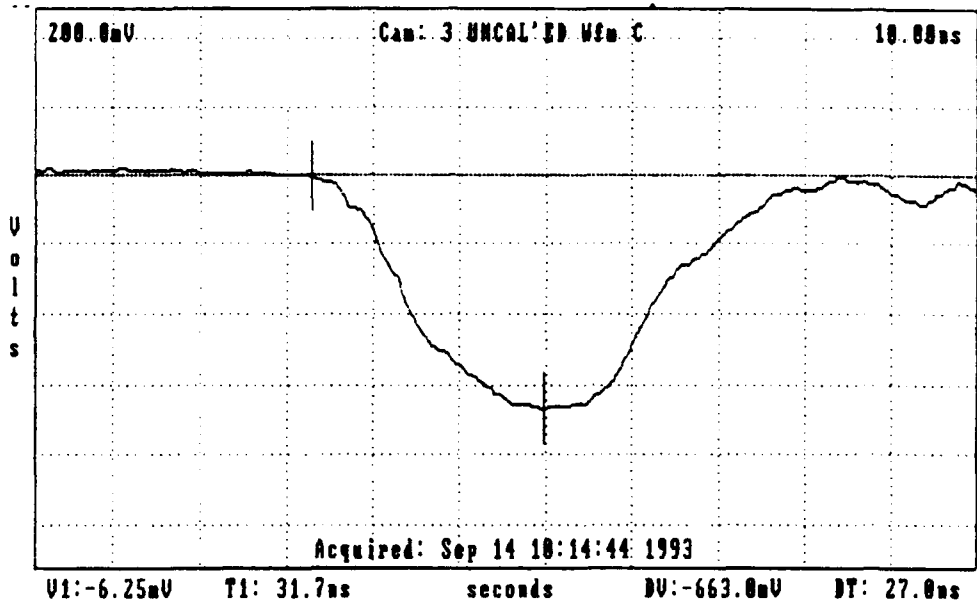


Figure 5.2 Diode Current 55kV.

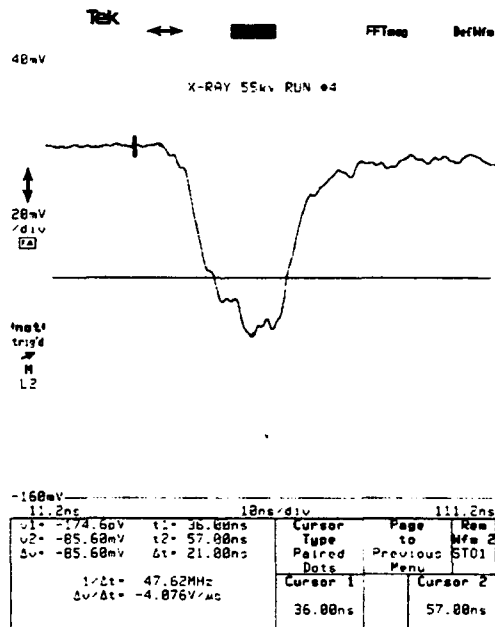


Figure 5.3 X-ray Signal 55kV. Note early slope changes. Diode voltage onset is marked at 28.9ns.

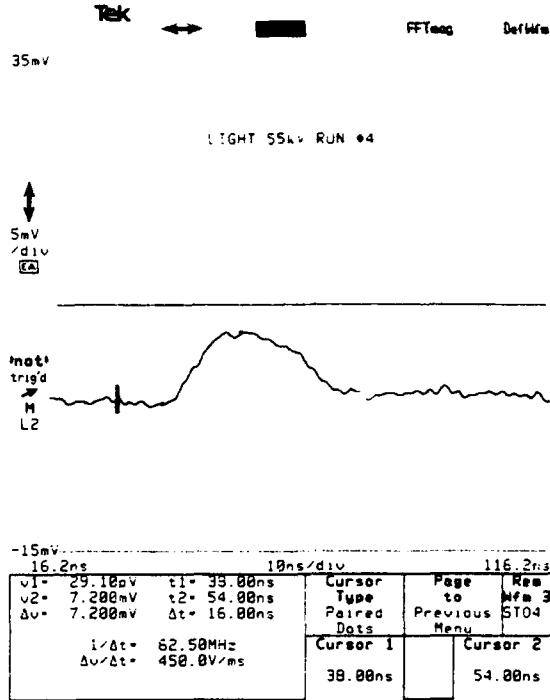


Figure 5.4 Cathode Light Signal 55kV. Diode voltage is marked at 28.9ns.

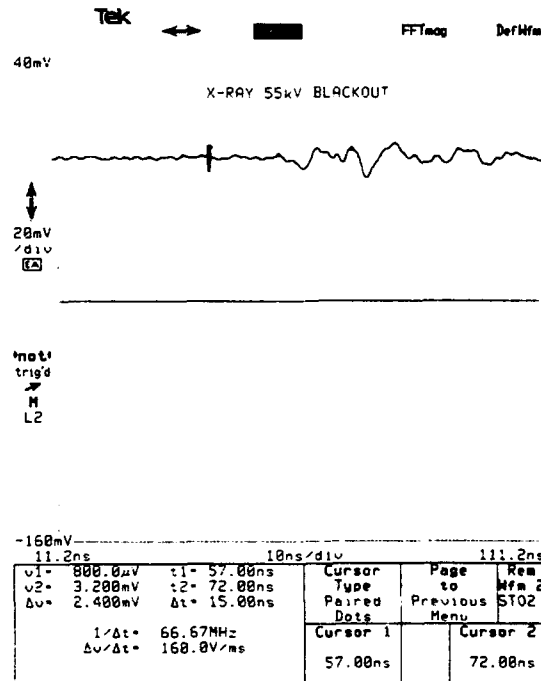
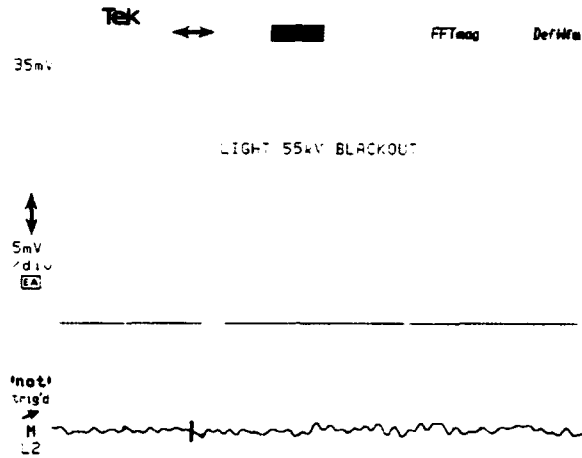


Figure 5.5 X-ray Blackout Signal 55kV. Voltage onset is marked at 42ns.



-15mV

16.2ns 10ns/div 116.2ns

v1= 29.10pV	t1= 29.00ns	Cursor Type	Page to	Res
v2= -800.0uV	t2= 44.00ns	Paired	Previous	Wfm 2
Δv= -800.0uV	Δt= 15.00ns	Dots	Menu	ST05
1/Δt= 66.67MHz		Cursor 1	Cursor 2	
Δv/Δt= -53.33V/ns		29.00ns	44.00ns	

Figure 5.6 Cathode Light Blackout Signal 55kV.

2. 75kV Examples

Figures 5.7 through 5.10 are examples from a typical 75kV shot. Figures 5.11 and 5.12 are blackout signals for the x-ray and light signals respectively.

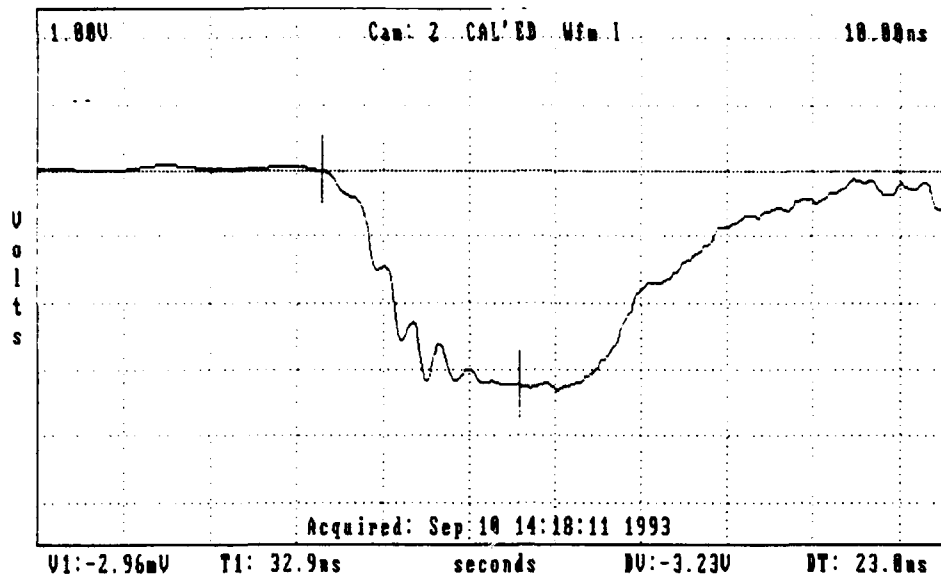


Figure 5.7 Diode Voltage 75kV. Note, noise on rising edge did not appear to affect plasma onset time.

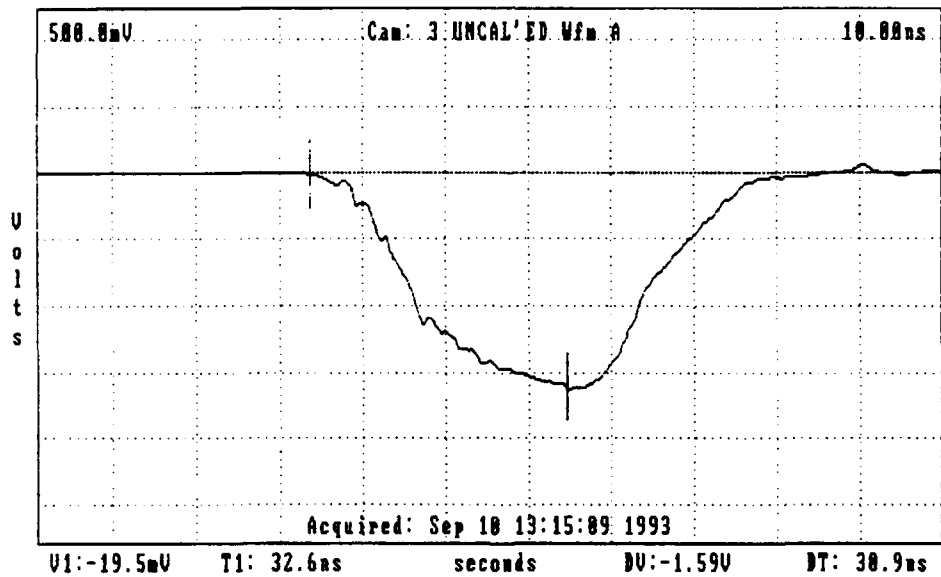


Figure 5.8 Diode Current 75kV. Ripples on rising edge correspond to voltage noise.

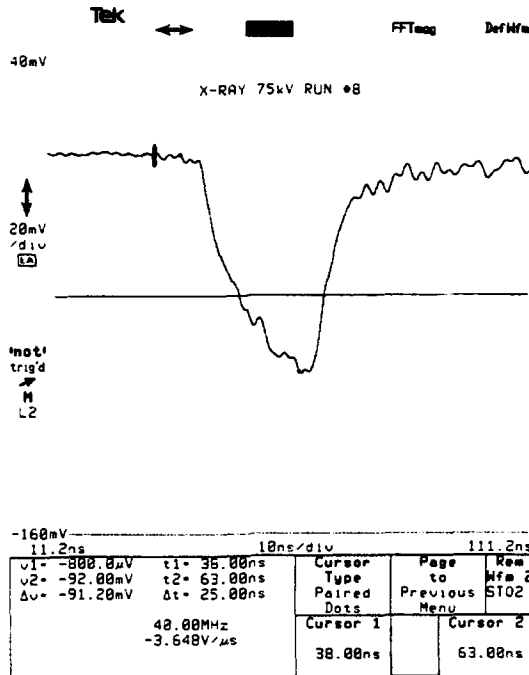


Figure 5.9 X-ray Signal 75kV. Note slow initial rise. Voltage onset is 32.9ns.

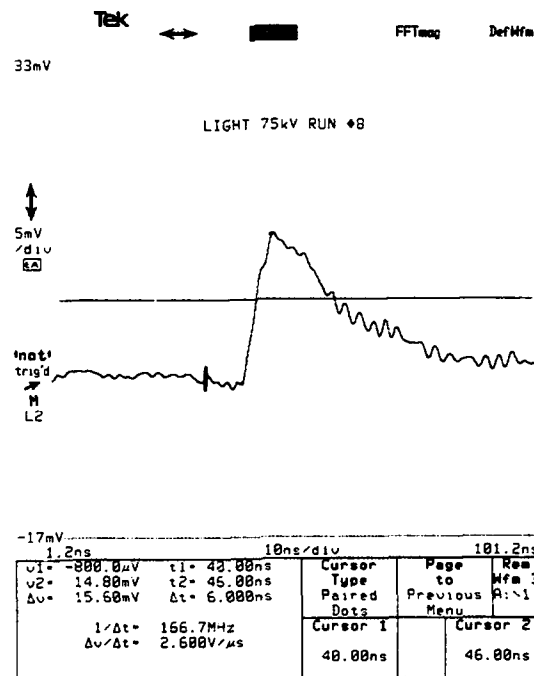
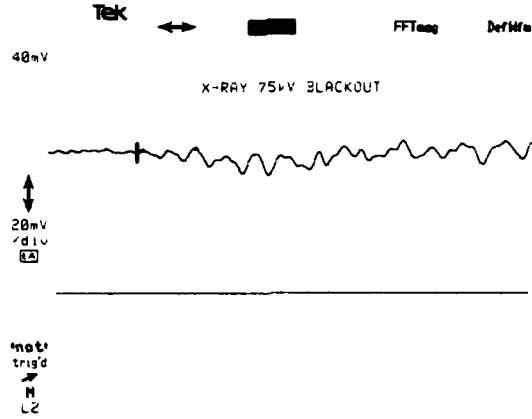


Figure 5.10 Cathode Light Signal 75kV. Note the rapid risetime.

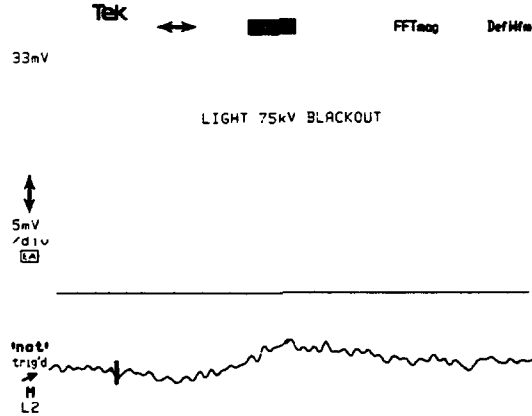


-160mV

11.2ns 10ns/div 111.2ns

v1 = -174.6mV	t1 = 30.00ns	Cursor Type	Page to	Rem
v2 = 800.0mV	t2 = 41.00ns	Paired	Previous	Mn 2
Δv = 800.0mV	Δt = 11.00ns	Dots	Menu	ST01
1/Δt = 90.91MHz		Cursor 1	Cursor 2	
Δv/Δt = 72.73V/ms		30.00ns	41.00ns	

Figure 5.11 X-ray Blackout Signal 75kV. Voltage onset is marked at 29ns; noise is not significant until 41ns.



-17mV

16.2ns 18ns/div 116.2ns

v1 = -349.2mV	t1 = 29.00ns	Cursor Type	Page to	Rem
v2 = 2.800mV	t2 = 65.00ns	Paired	Previous	Mn 2
Δv = 2.800mV	Δt = 37.00ns	Dots	Menu	A:1
27.03MHz		Cursor 1	Cursor 2	
75.68V/ms		28.00ns	65.00ns	

Figure 5.12 Cathode Light Blackout Signal 75kV. Voltage onset marked at 29.2ns.

3. 100kV Examples

The 100kV examples are the most problematic. Conclusions drawn from these examples must be made with healthy skepticism due to noise problems with the x-ray signal, and timing problems with the current. Figure 5.13 shows the diode voltage with an easily discernible onset.

Figure 5.14 Shows the diode current. The onset is ambiguous, and even selecting the latest possible onset, it starts 5ns before the voltage. the noise spike on the leading edge corresponds to the voltage onset time.

Figure 5.15 shows the x-ray signal. The x-ray signal is plagued by EM noise at the onset, so the true onset of the x-rays is difficult to determine.

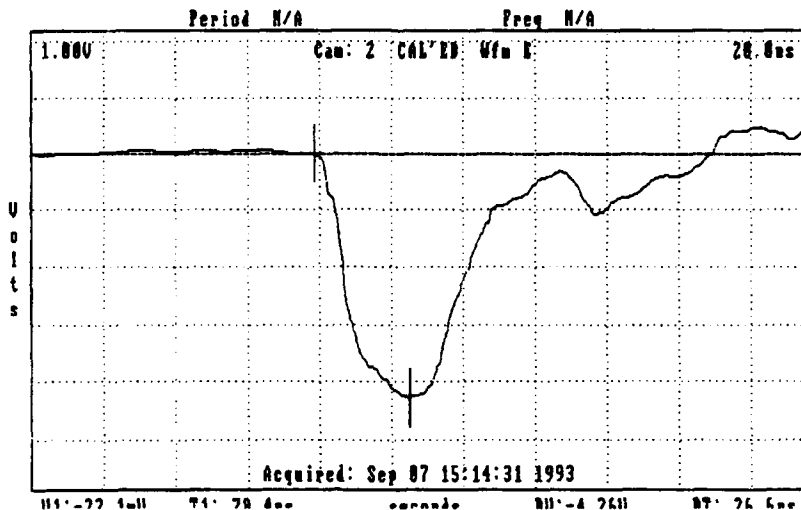


Figure 5.13 Diode Voltage 100kV.

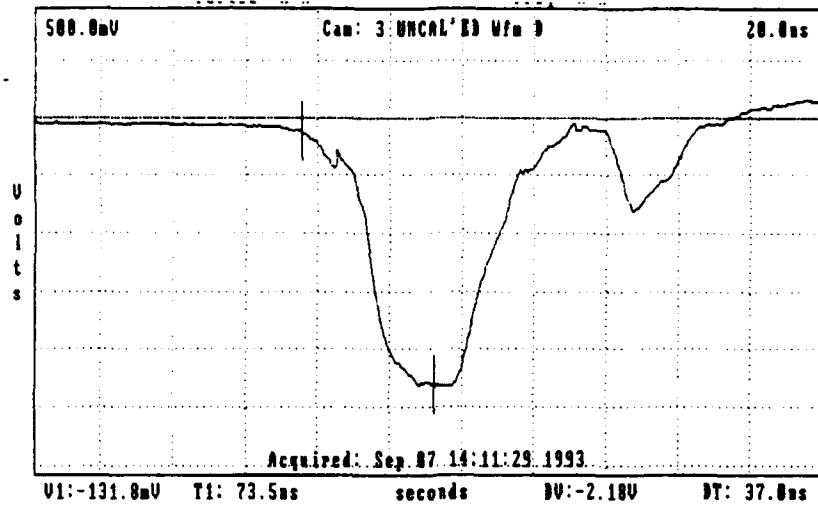


Figure 5.14 Diode Current 100kV. The early noise spike occurs simultaneously with voltage onset.

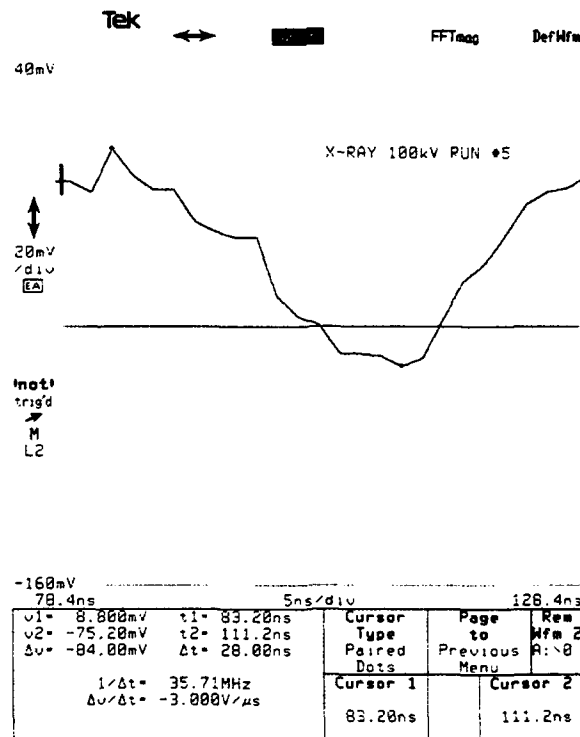


Figure 5.15 X-ray Signal 100kV. Noise spike at onset time matches noise onset for the blackout signal.

Figure 5.16 shows the cathode light signal with a more gradual rise for the first 2ns then a very dramatic rise. This may have significance in the plasma build-up and onset of breakdown.

Figures 5.17 and 5.18 are the 100kV blackout signals. In both cases, the noise signals onset near the signal onset times if the voltage is used as a reference or start time (see 100kV spreadsheet in Appendix A.)

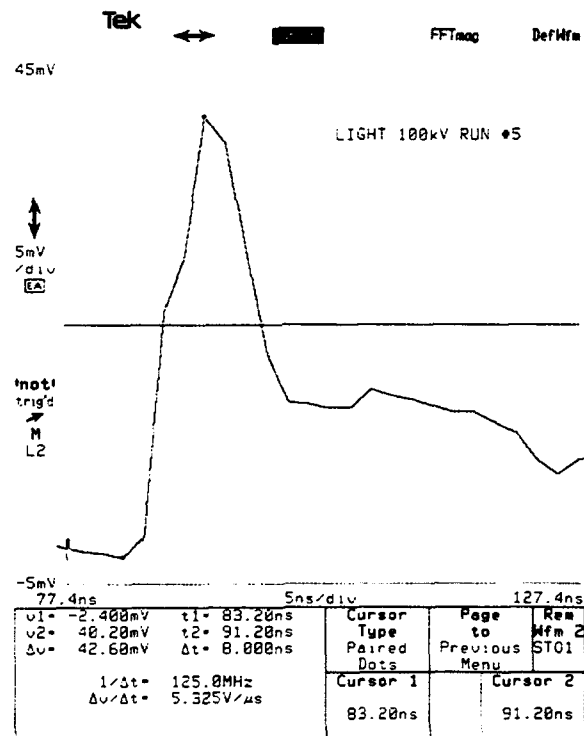
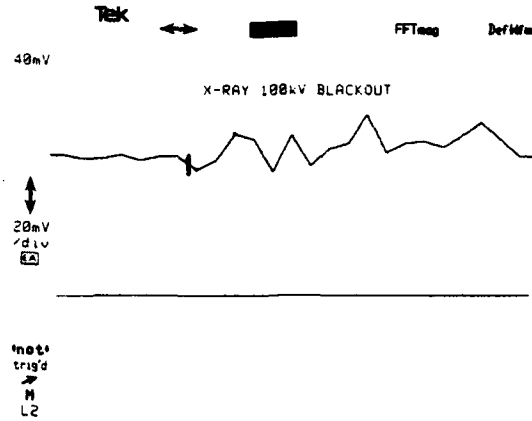


Figure 5.16 Cathode Light Signal 100kV. Note change in slope 2ns after initial rise.

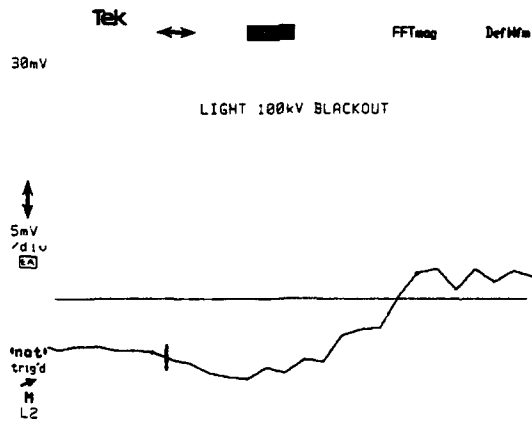


-160mV

63.4ns 5ns/div 113.4ns

v1 = -7.200mV	t1 = 79.20ns	Cursor Type	Page to	Rem
v2 = 8.800mV	t2 = 82.20ns	Paired	Previous	Mfn 2
Δv = 15.20mV	Δt = 4.000ns	Dots	Menu	A: \0
1/Δt = 250.0MHz		Cursor 1	Cursor 2	
Δv/Δt = 3.800V/μs		79.20ns	82.20ns	

Figure 5.17 X-ray Blackout Signal 100kV.



-20mV

64.4ns 5ns/div 114.4ns

v1 = -503.9μV	t1 = 74.80ns	Cursor Type	Page to	Rem
v2 = 7.796mV	t2 = 102.8ns	Paired	Previous	Mfn 2
Δv = 8.400mV	Δt = 28.00ns	Dots	Menu	ST03
1/Δt = 35.71MHz		Cursor 1	Cursor 2	
Δv/Δt = 300.0V/ms		74.80ns	102.8ns	

Figure 5.18 Cathode Light Blackout Signal 100kV.

B. Superimposed Digitized Waveforms

The signals captured by both the DCS and the DSA can be converted to spreadsheets and plotted on the same graph. This is helpful for comparing the timing information. Since the voltage values of the signals differ, it is best to scale the waveforms. Scale factors for the waveform are noted with each figure. Figure 5.19 shows the entire pulse for one of the 55kV shots. This gives an overview of how the signals "follow" the voltage. Figure 5.20 is a blow-up of the same pulse showing the onset.

Figure 5.21 shows the whole pulse for a typical 75kV shot. The x-ray signal onset is 38ns. Figure 5.22 shows the onsets of all signals.

Figures 5.23 and 5.24 show the 100kV full pulse and onset respectively. The current onsets before the voltage. We attribute this to experimenters error. The noise in the x-ray signal corresponds to the onset of noise in the blackout, making onset determination more difficult.

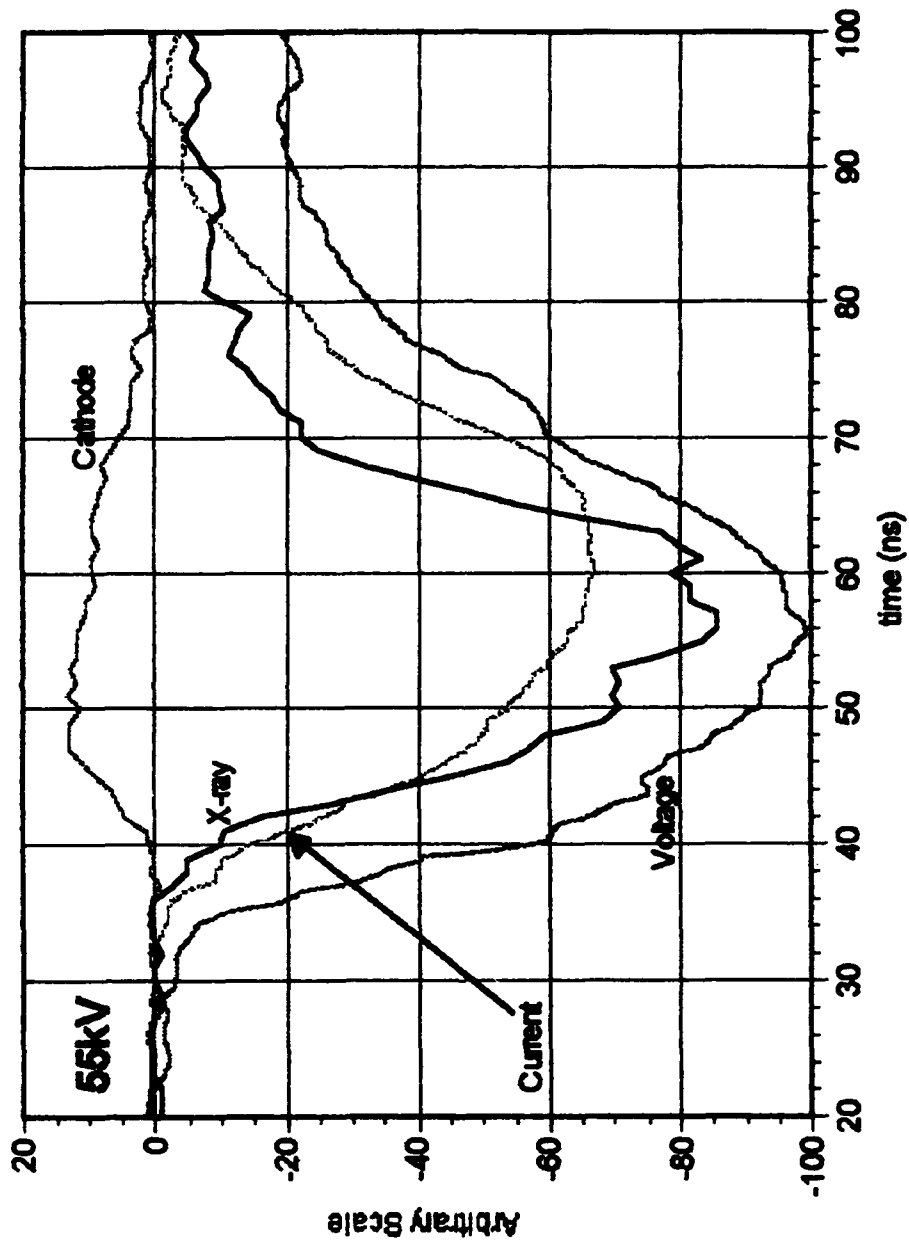


Figure 5.19 55kV Full Pulse. Note rapid x-ray pulse rise. Scale factors: Voltage (50x); Current (100x); Cathode (2000x); and X-ray (1000x).

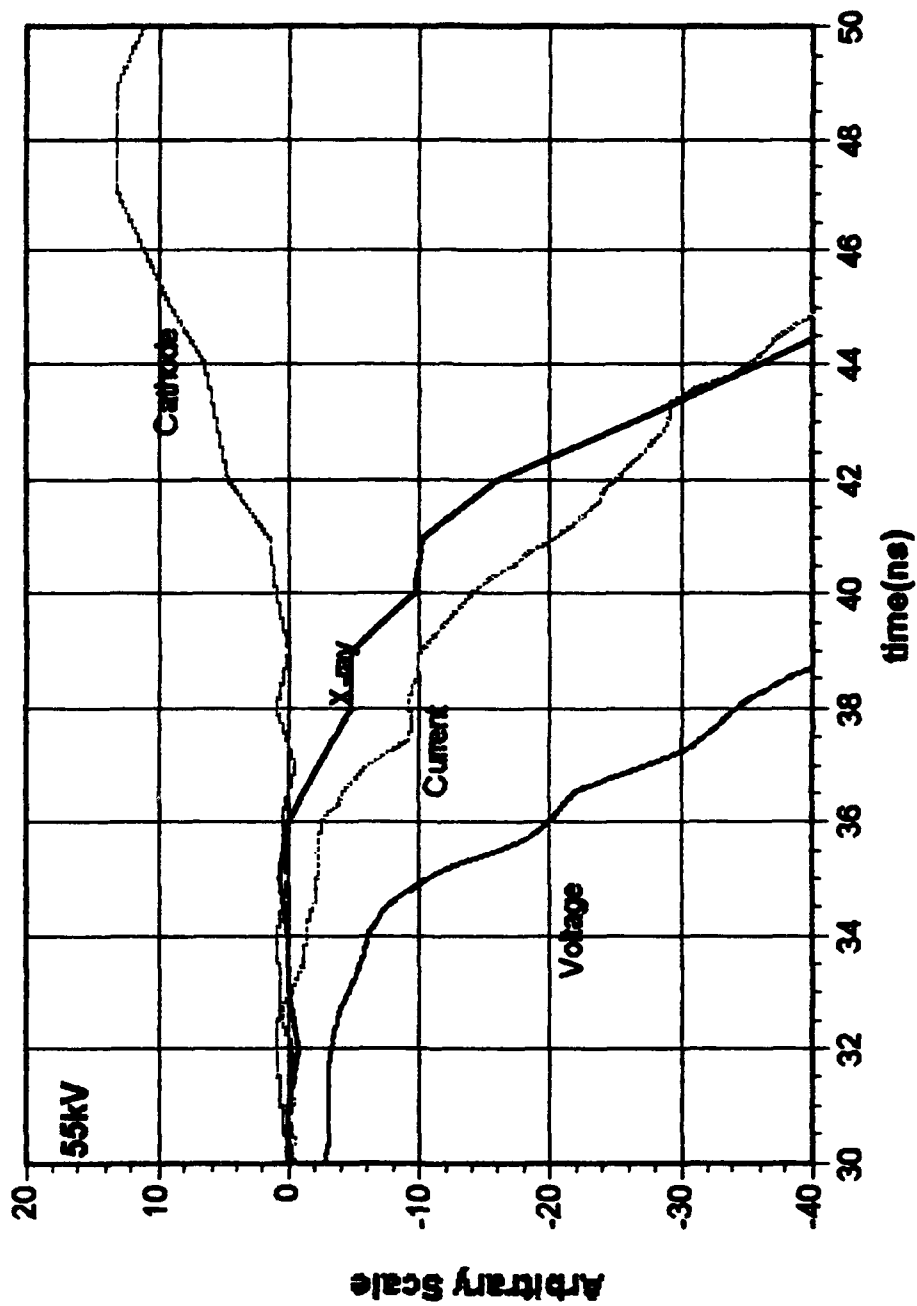


Figure 5.20 55kV Onset. Note rapid rise in x-ray signal at cathode onset. Scale factors same as Fig. 5.19.

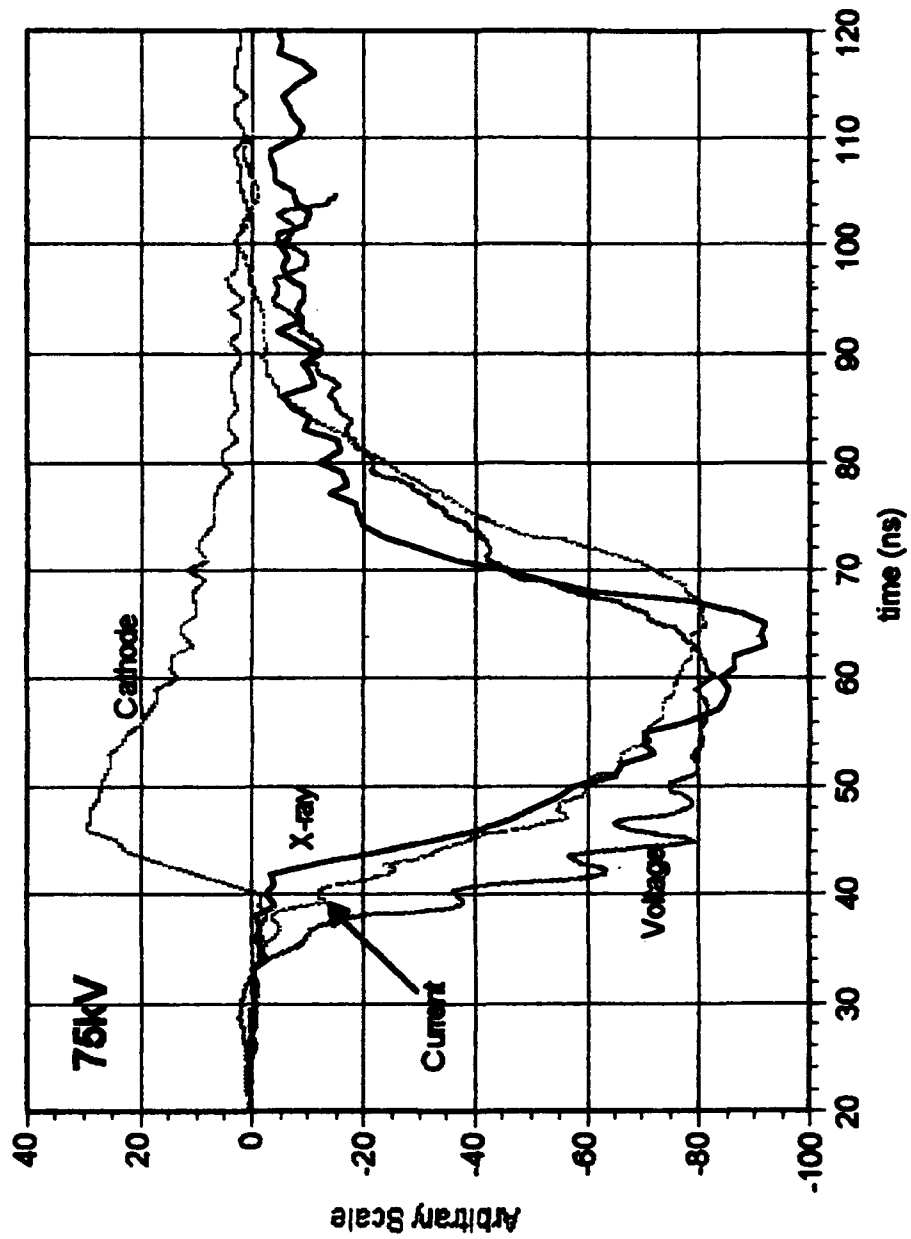


Figure 5.21 75kV Full Pulse. Note how current follows voltage. Scale factors: Voltage (25x); Current (50x); Cathode (2000x); and X-ray (1000x).

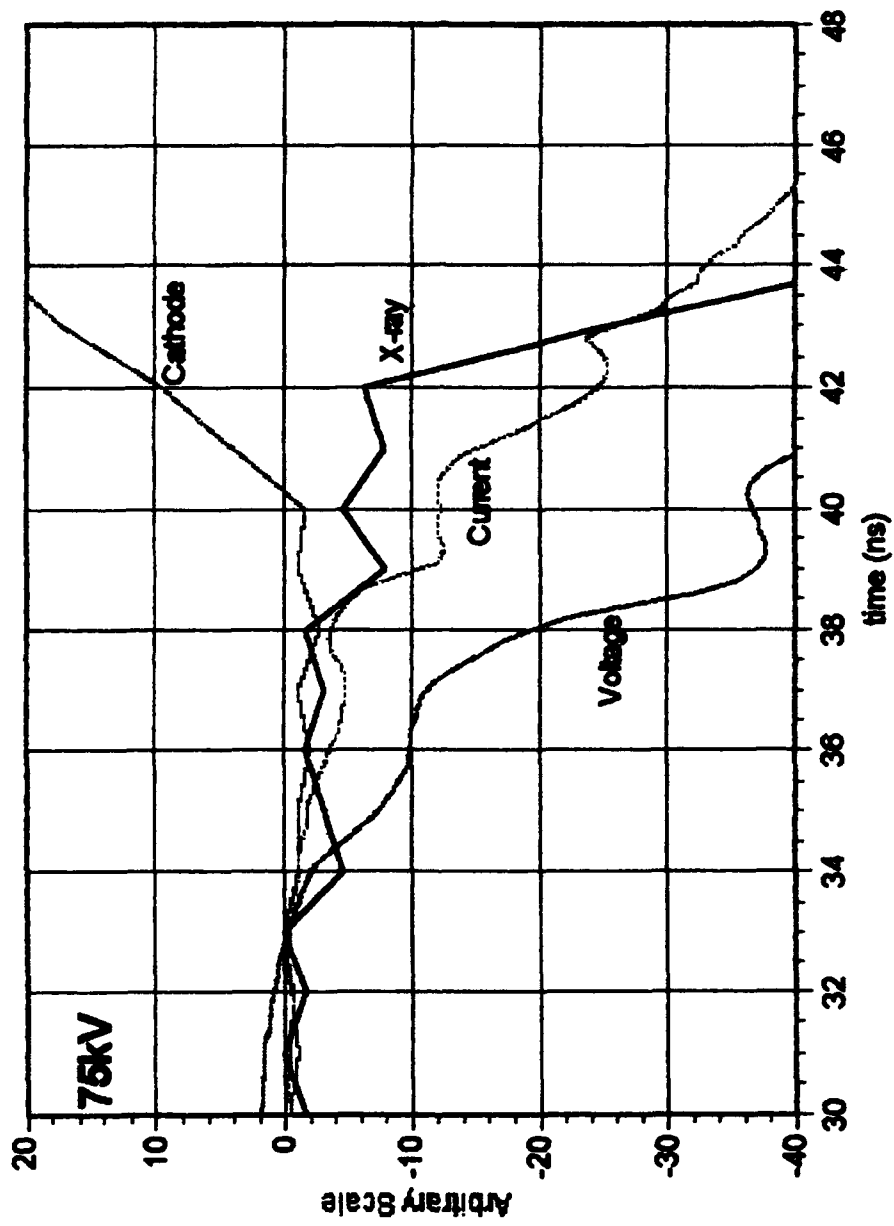


Figure 5.22 75kV Onset. X-ray Signal is scaled 2X from Fig 5.21.

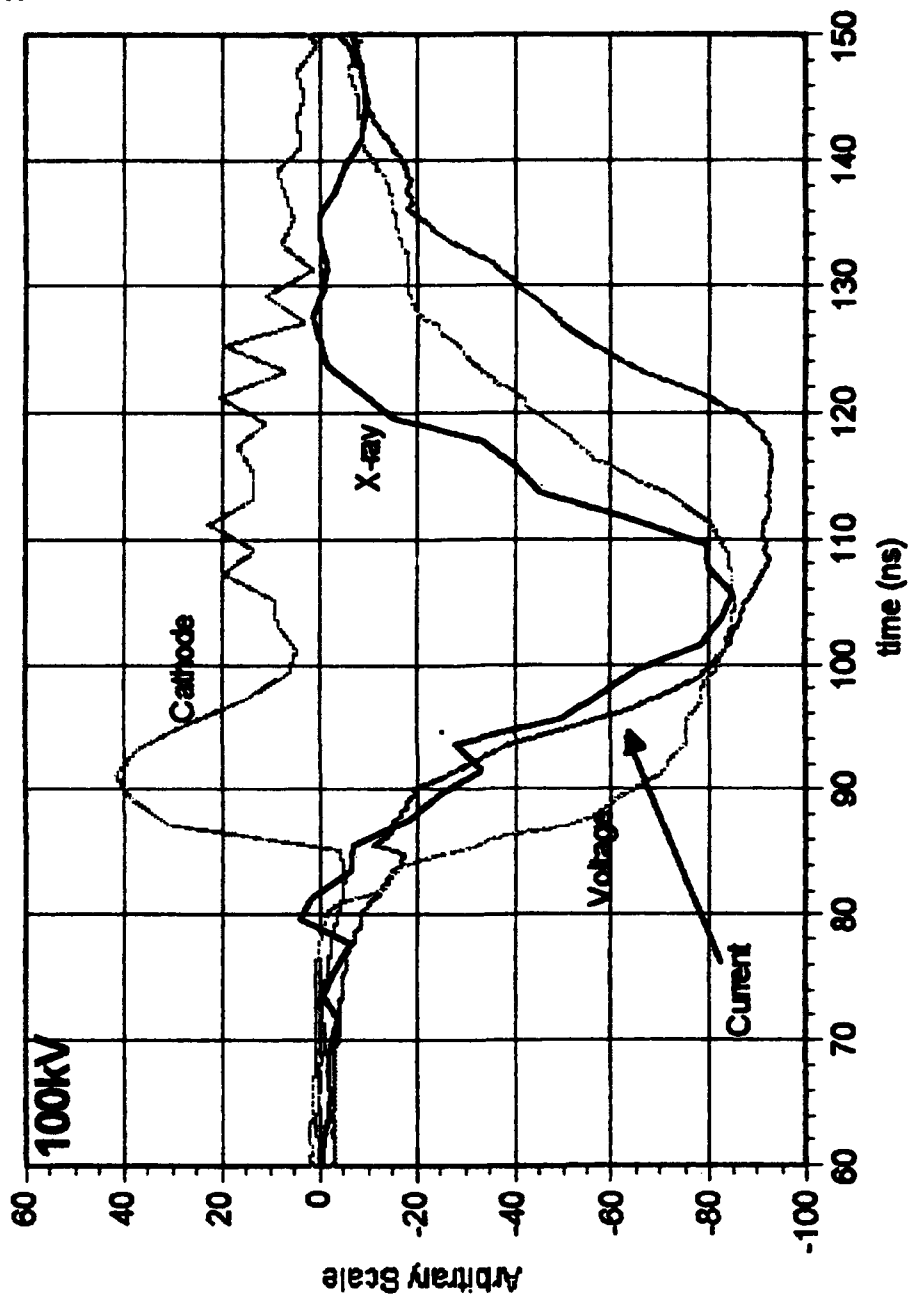


Figure 5.23 100kV Full Pulse. Note current appears to onset before voltage. Scale factors: Voltage (25x); Current (40x); Cathode (2000x); and X-ray (1000x).

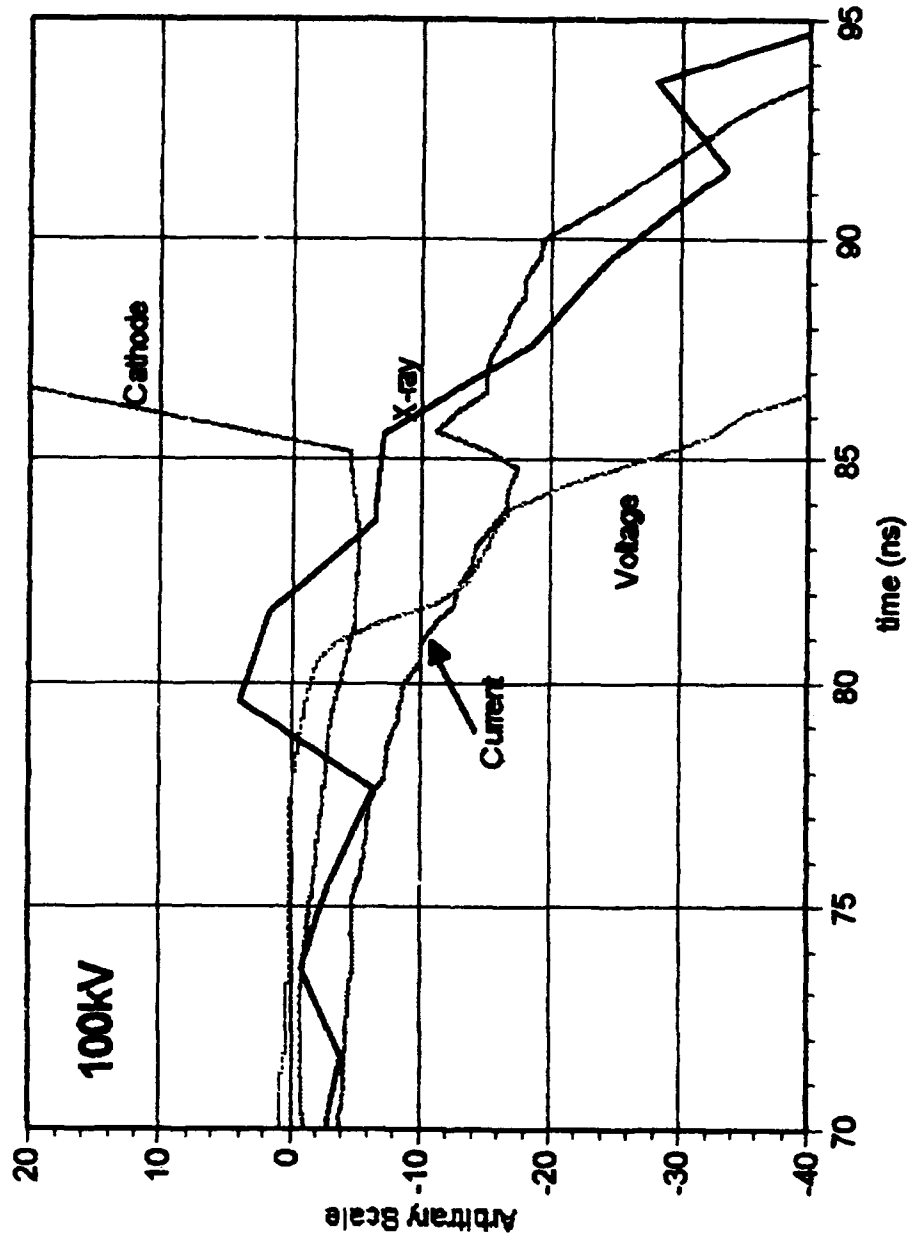


Figure 5.24 100kV Onset. Note noise spike in x-ray signal. Scale factors same as Fig. 5.23.

C. Average Onset Times

Ten data shots were done for each Marx voltage. These groups of ten were considered as data sets, and average onset times were determined for the parameters measured. Using the diode voltage onset as the zero of time, I calculated the delays before current, x-ray and cathode light onset. Additionally, I determined the voltage at which x-ray production began. Table 5.1 shows the average values for the three data sets. The raw times for each data run are in Appendix A.

Table 5.1 AVERAGE DELAY TIMES FROM VOLTAGE ONSET (TEN SHOTS AT EACH VOLTAGE); AND VOLTAGE AND ELECTRIC FIELD AT X-RAY ONSET

Marx Voltage	Delay Times* (± 1.2 ns) From Voltage Onset (ns)			X-ray Onset	
	Current	X-ray	Cathode Light (Plasma)	Diode Voltage (kV)**	Electric Field (MV/m)
55	2.2	6.93	10.33	179 \pm 54	7.08
75	0.09	5.13	6.58	256 \pm 125	10.1
100	-2.72	5.16	5.86	226 \pm 230	8.92

* Note $t_0=0$ is voltage onset.

** These values are \pm error factors as determined in Appendix B.

VI ANALYSIS

A. COMPARISON OF ACTUAL AND PREDICTED PLASMA ONSET

Based on the model presented in Chapter III, the onset of plasma formation can be predicted by plotting the distance of the 100V EPS from the cathode using actual data from the voltage curves, and the desorbed neutral distance from the cathode assuming $V=470\text{m/s}$. [Ref. 3] This velocity is the average velocity of air molecules at 300°K expanding into a vacuum [Ref. 8]. Figures 6.1 through 6.3 show these plots for the three different Marx voltages.

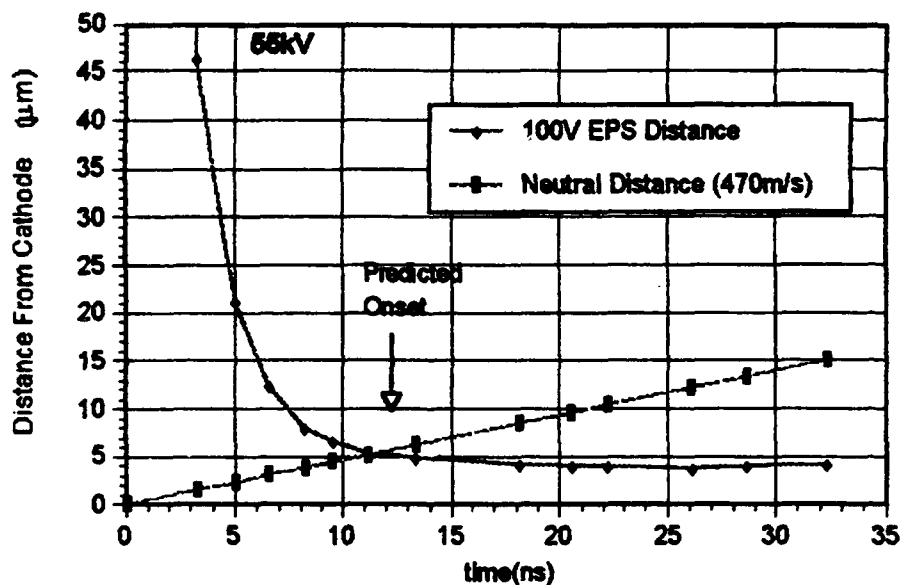


Figure 6.1 Distance of 100v EPS and Neutrals From the Cathode(55kV). Delay of plasma formation from voltage onset =11.5ns.

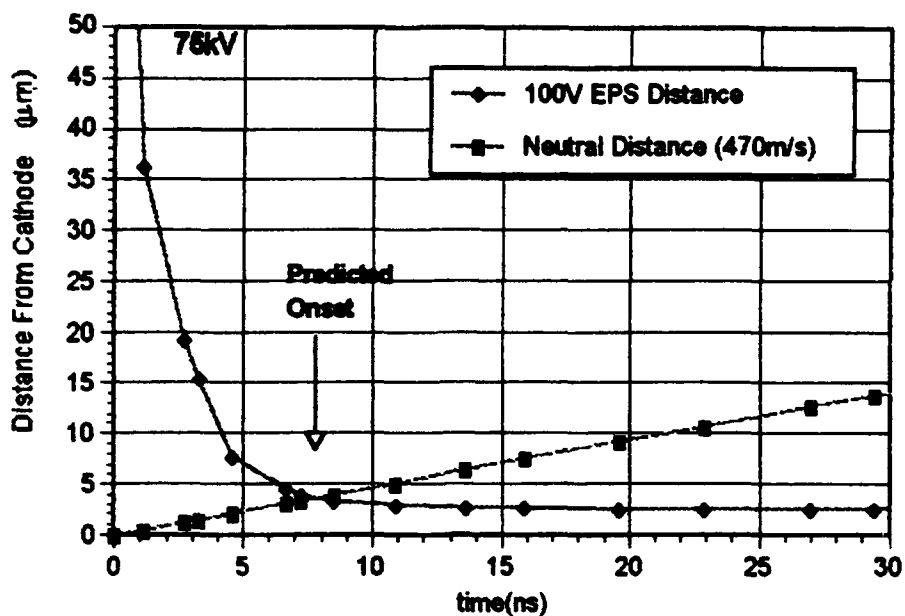


Figure 6.2 Distance of 100v EPS and Neutrals From the Cathode(75kV). Delay of plasma formation from voltage onset =7.5ns.

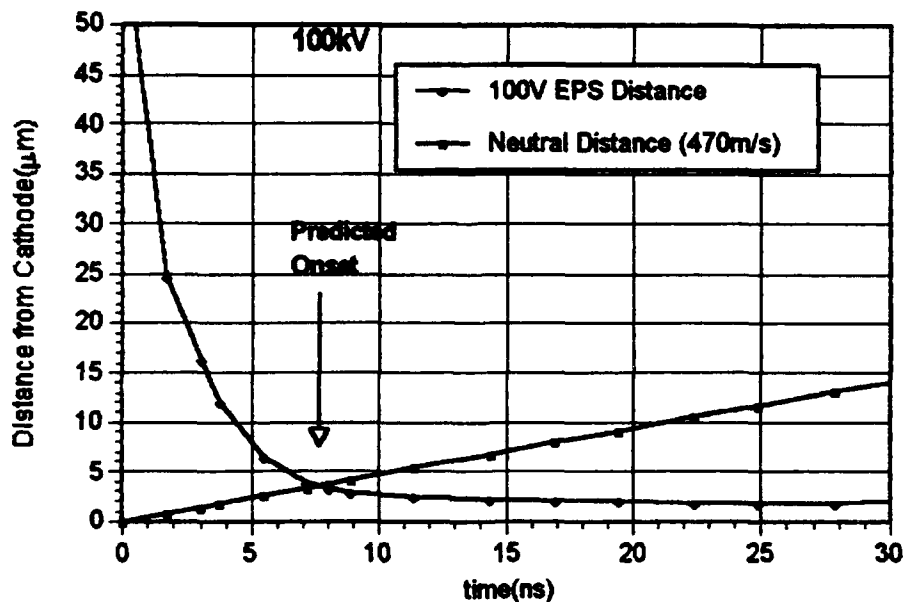


Figure 6.3 Distance of 100v EPS and Neutrals From the Cathode(100kV). Delay of plasma formation from voltage onset =7.5ns.

To see how these values compare to those obtained in the experiment, and get an overall view of the process, I set up the time lines in Fig. 6.4 using the average onset times from Table 5.1.

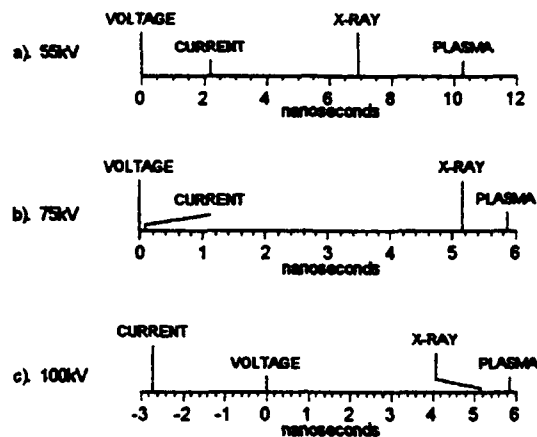


Figure 6.4 Plasma Formation Time Sequence.

These plasma onset times agree very favorably with the prediction, considering the ± 1 ns timing resolution of our experiment (see Appendix B for error analysis of time resolution). Both Hallal, [Ref. 3] and Wright [Ref. 10] cover this plasma formation in great depth, and I will now move on to discuss how the x-ray signal fits into the picture.

B. X-RAY ONSET

1. Overview

Based on the DNI model, one expects that field emission will begin when the macroscopic electric field,

$E=10\text{MV/m}$ ($\beta=100$) and that this electron current will register as an x-ray signal due to bremsstrahlung and excitation at the anode. The diode current signal will have some initial rise from the displacement current, so the x-ray signal is the best measure of when field emission begins. If the DNI model is correct, we would see a small x-ray signal at $E=10\text{MV/m}$ that begins the ionization, followed shortly by plasma formation and rapid rise in the x-ray signal due to thermionic emission and the unipolar arc electrons. This effect is seen in all the example waveforms (see Figs. 5.19-5.24) and in most of the data. The x-ray signal starts with a shallow slope, until the plasma formation begins, then the x-ray signal (electron current) rises very rapidly. Even in cases where the x-ray signal rises rapidly at first, its magnitude is very small at the plasma onset time. In most of the 100kV cases, the initial slow rise is masked by a positive noise spike.

2. Displacement Current

The current detector always registers a current before the onset of x-rays. The x-ray detector is the most accurate way to see the onset of the convection electron current. The question now is; where does the initial current reading come from? A simple calculation of the displacement current can provide the answer.

The displacement current density (j_D) for the diode prior to field emission is given by:

$$j_D = \epsilon_0 \frac{dE}{dt} \quad (6.1)$$

Using Equation 2.1 and assuming negligible space charge effect (before field emission) Eq. 6.1 becomes:

$$j_D = \frac{\epsilon_0}{d} \frac{d\Phi}{dt} \quad (6.2)$$

Using an example from our experiment; $d=2.5\text{cm}$, and $d\Phi/dt=160\text{kV/ns}$ (from Fig. 5.7 and Eq. 4.1) Equation 6.2 gives $j_D \approx 6\text{A/cm}^2$ at $t=5\text{ns}$ after voltage onset. From Figure 5.8 and Eq. 4.2, the total current at that time is $I_{\text{tot}} \approx 730\text{A}$. Assuming an effective area for the diode of 20cm^2 [Ref. 3] then $I_D \approx 120\text{A}$, a significant but not overwhelming part of the total. If one considers the field enhancement factors, and their effect on the displacement current, an enhanced displacement current (j_{DE}) can in fact account for most of this initial current. Using an enhancement factor $\beta=100$, then, $j_{DE} \approx 600\text{A/cm}^2$. If this enhancement affects only 5% of the total area then $I_{DE} \approx 600 + 114 = 714\text{A}$, nearly the total current registered. The argument for the enhancement factor $\beta=100$ is well established in the literature [Refs. 2,6]. It is the rapidly changing electric field that accounts for the initial current rise, not a large electron current. This validates the idea that the x-ray detector is the best measure of the convection electron current.

3. Field Emission and Enhanced Field Emission

It is well established that field emission of electrons turns on when the local electric field $\approx 10^6 \text{V/m}$ [Refs. 2,6]. It is also accepted that electric field enhancement factors of $\beta=100$ are common [Ref. 6]. The values of E at x-ray onset from Table 5.1 using $\beta=100$ agree very closely with this threshold (10^6V/m) value. This initial field emission seems to be small however, and does not rapidly build until the onset of plasma formation. This can be explained by the unipolar-arc theory [Ref.7]. As the field emission begins, the neutrals begin to be ionized and the ions impart their kinetic energy into the surface layers of the cathode. Additionally, the ions enhance the electric field above the forming cathode spot increasing the field emission current through the FN equation (Eq. 3.2). These processes rapidly heat the spot area allowing plasma formation and thermionic emission of electrons [Ref. 6]. These electrons then provide the source for the high electron current and consequently, the increase in the x-ray signal. The initial field emission is from single points, and is rather small. Once the plasma spreads over an appreciable area of the cathode, the emission of electrons from the dense plasma created by the unipolar arc provides the high current across the diode gap.

C. LIMITATIONS OF INTERPRETATION

There are several assumptions that must be clarified in the context of the data to bring about a complete understanding of the process.

1. Child-Langmuir Current Limitation

One of the assumptions of this model is the planar diode assumption. This assumption stated mathematically is:

$$\frac{r_c}{d} \gg 1$$

where r_c is the cathode radius, and d is the diode spacing. At first glance, this appears not to apply to the NPS FXR diode. In fact, we are actually looking at the cathode as many small area electron emitters, i.e. from whiskers ($\sim \mu\text{m}$) and dust particles ($\sim 10\mu\text{m}$). Welsh [Ref. 4] did a simulation using whisker parameters and determined that the current was in fact Child-Langmuir limited within a given flux tube.

2. X-ray Detector Efficiency

The detector used to record the x-ray signal was not designed specifically for this purpose, so it is important to know how the detector will respond in the energy range we are using. The most important electron energy range for our purpose was between 100 and 200keV, near the onset of field emission. Figure 6.5 shows a sample efficiency of detectors out to 500kV. Based on the detector placement trials (Chapter IV) where saturation of the detector occurred inside a certain distance from the anode, there are enough photons produced to

overcome the drop-off in efficiency. The fact that the detector begins to give a signal at approximately 10MV/m adds further to my confidence that it is the best measure of the electron current.

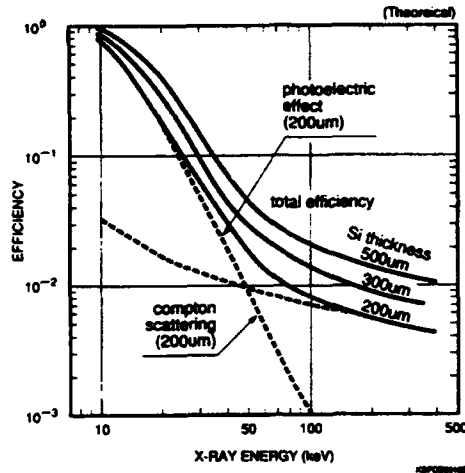


Figure 6.5 Detection Efficiency of Silicon Detectors. [Ref. 18]

3. Relativistic Considerations

In this study we deal only with the plasma formation mechanism at the cathode. This mechanism acts over a distance of about 50 μ m from the cathode, where the electrons are not yet relativistic. In short, relativity is not important to the cathode process.

The electrons become relativistic before striking the anode, but the relativistic effects are minimal [Ref. 3] and do not effect the x-ray production process.

4. Electromagnetic Noise

EM noise is a major consideration in the interpretation of this data. Hundreds of trial firings were

done to reduce noise, increase signal to noise, and determine detector placement. Knowledge gained from these firings, and proper use of the blackout signals serves to validate the interpretations presented. The blackout signals are especially important, but they must be compared to the signals using the onset of voltage as the zero of time. Even with the noise problems, the rapid increases in the signals were easy to determine although the initial slow rises are more difficult to predict.

VII CONCLUSION AND RECOMMENDATIONS

A. CONCLUSION

The explosive electron emission model requires a much higher current density than allowed by the Child-Langmuir law. The DNI model provides a mechanism that efficiently delivers the energy required to form cathode spots. This study confirms the temporal character of the DNI model, and provides an explanation for the electron current behavior.

The data from this experiment shows that the x-ray onset occurs before the cathode plasma (light) onset for all voltages. It also shows that the x-ray onset occurs at approximately the same diode electric field value (10MV/m) for all of the voltages. Finally, it shows that the x-ray signal increases dramatically at the plasma onset time.

The plasma onset times obtained in this experiment agree favorably with the model prediction, and the previous work of Hallal [Ref. 3]. The only real substantive change to the theory for this work was to use a faster neutral expansion velocity (470m/s) that is the average velocity of air molecules at 300°K. The primary thrust of this experiment was to measure the x-ray signature and hence the electron current. Applying the electric field enhancement factor, β , to the displacement current explains the initial rise in the current. Then using an x-ray detector we can detect onset of the

electron current. The x-ray signal starts when the enhanced electric field reaches 10^9 V/m as expected, for the start of field emission. The initial signal is small until plasma formation begins. The rapid rise in the x-rays at the time of plasma formation is due to the onset of breakdown and plasma formation on the cathode surface by unipolar arcing which provides an ample source of electrons for the x-rays. The entire process develops on a nanosecond time scale because the limiting time is the relatively slow, several nanosecond flight time of the neutrals to the ionization region. Once ionization begins, the process develops rapidly due to the relatively short flight times of both the ions (10^{-10} s) to the cathode surface and electrons (10^{-13} s) from the cathode to the ionization region, a few μm away from the cathode surface.

B. RECOMMENDATIONS

There are several improvements to this experiment and some new experiments that could provide further insight into this model. Improvements to this experiment would include using more sensitive diode current and voltage detectors and an x-ray detector with a known thickness and better noise immunity. Firing at lower voltages should lengthen the delay time; this could provide a better contrast for verification of the model. Lower voltages should also see a longer delay between x-ray onset and plasma formation because of the slower movement of the 100V EPS.

A new experiment that would help confirm the desorption of neutrals would be one that coats the cathode with contaminants and checks their predicted flight time against the plasma formation time [Ref. 3]. An additional experiment to check the field emission current could include using an x-ray detector with sensitivity to low energy x-rays placed inside the vacuum chamber to see the initial signal better and check if the aluminum back plate on the anode is stopping any initial low energy x-rays.

APPENDIX A: DATA

The primary data collected for this experiment was the onset time of the signals for diode voltage, diode current(I), cathode light(C), and x-rays(X). Additionally, the diode voltage at the time of x-ray onset was determined and recorded for each run. Tables A.1, A.2, and A.3 show the data for the 55kV, 75kV, and 100kV data sets respectively.

The first column of each table gives the run number. Run #11 is the blackout run for each voltage. Columns 2 through 5 show the raw times for each onset as measured by the DCS/DSA. Columns 6 through 8 compare the differences in onset times of each signal to the onset time of the voltage. Column 9 shows the difference between the x-ray and current onset. All times are in nanoseconds.

The last column in each table indicates the oscilloscope trace voltage that represents the diode voltage at x-ray onset time. Convert the trace voltage to an actual voltage using Equation 4.1, and determine the electric field with Equation 2.1.

Table A.1 55kV DATA

55kV DATA										
RUN#	VOLTAGE (V)	CURRENT (I)	X-RAY (X)	CATHODE (C)	I-V	X-V	C-V	X-I	Volts at X Onset	
1	23	27.2	31.5	35	4.2	8.5	12	4.3	0.54	
2	22.6	27.4	31	36	4.8	8.4	12.4	3.8	0.279	
3	30.3	33.6	37	41	3.2	6.7	10.7	3.5	0.325	
4	28.9	31.7	35.5	39	2.8	6.8	10.1	3.8	0.323	
5	35.5	37.6	42	45	2.1	6.5	9.5	4.4	0.58	
6	38.6	41	46.5	50	2.4	7.9	11.4	5.5	0.84	
7	43.3	44.3	49	62.5	1	5.7	9.2	4.7	0.67	
8	43.1	43	49.5	53	-0.1	6.4	9.9	6.5	0.76	
9	42.7	42.8	49.5	52	0.1	6.8	9.3	6.7	0.835	
10	44.2	45.7	50	53	1.5	5.8	8.8	4.3	0.79	
11	42.1	42.6	58	60	0.5	15.9	17.9	15.4		
Averages					2.2	6.93	10.33	4.73	0.5622	
							Potential (KV)		180	
							Electric Field (V/m)		7.08E+08	

Table A.2 75kV DATA

75kV DATA										
RUN#	VOLTAGE (V)	CURRENT (I)	X-RAY (X)	CATHODE (C)	I-V	X-V	C-V	X-I	Volts at X Onset	
1	33.9		38	39	0.6	4.1	5.1	7.2	0.508	
2	29.2	28.8	37	37	0.3	7.8	7.8	4.3	1.48	
3	32.9	33.2	37.5	38	0.4	4.8	5.1	4.7	0.728	
4	30.9	31.3	36	39	0.1	6.1	8.1	5.8	0.585	
5	31.1	31.2	37	38	-0.7	5.9	6.9	6.8	1.27	
6	24.4	23.7	30.5	31	-0.2	6.1	6.6	3.7	1.2	
7	31.5	31.3	35	38	-0.3	3.5	6.5	5.4	0.432	
8	32.9	32.6	38	40	0.2	5.1	7.1	4.8	0.774	
9	32	32.2	37	39	-0.1	6	7	4.2	0.454	
10	31.4	31.3	35.5	37	0.6	4.1	5.8	5.2	0.619	
11	29.2	29.8	35	38	NA	5.8	6.8			
Averages					0.09	6.13	6.58	5.21	0.6028	
							Potential (kV)		257	
							Electric Field (V/m)		1.01E+07	

Table A.3 100kV DATA

100kV DATA										
RUN#	VOLTAGE (V)	CURRENT (I)	X-RAY (X)	CATHODE (C)	I-V	X-V	C-V	X-I	Volts at X Onset	
1	74.6	73.4	78.8	79	-1.2	4	4.4	5.2	0.608	
2	83.9	83.9	80.6	80.6	0	6.7	6.7	6.7	1.08	
3	77.2	73.5	81.4	81.8	-3.7	4.2	4.6	7.8	0.648	
4	78	76.5	83.4	85.6	-1.5	6.4	7.6	6.9	0.595	
5	78.4	77.8	83.6	84	-0.6	5.2	5.8	5.8	0.805	
6	75	70	80	81.4	-5	5	6.4	10	0.57	
7	78.4	74.8	83.8	84.4	-3.8	5.4	6	9	0.775	
8	75.3	73	81	80.6	-2.3	5.7	5.3	8	0.74	
9	76.3	72.2	81.8	82	-4.1	5.5	5.7	9.6	0.748	
10	78.1	70.9	80.6	82.4	-5.2	4.5	6.3	9.7	0.535	
11	77.6	70.4	76.2	74.8	-7.2	-1.4	-2.8	6.8		
Average					-2.72	6.16	6.86	7.88	0.708	
									Potential (kV)	227
									Electric Field (V/m)	8.82E+08

APPENDIX B: ERROR ANALYSIS

A. TIME MEASUREMENTS

This section explains the timing error calculations used in the results and analysis chapters of this report. The sources of error are divided into two categories. The first being those that are compensated for by the synchronization procedures outlined in the experiment section including time base errors of the oscilloscopes and DSA's and electrical signal travel time. These timing differences are resolved to within 0.3 ns of error. This, along with the other category of uncontrollable independent error are listed below in Table B.1 below.

Table B.1 TIMING ERROR

1.	Synchronization	0.3ns
2.	Oscilloscope (3% X 10ns) with 7B92A	0.3ns
3.	Digitizing Signal Analyzer (0.03% X 10ns)	0.03ns 1ns res*
4.	Digital interpretation by DCS	0.1ns
5.	Digital interpretation by DSA	0.1ns
6.	Delay Generator	0.5ns

* Though the accuracy is 0.03%, data points are only taken every nanosecond so worst case error is actually 1 ns.

These errors are all independent so they can be added in quadrature. The resulting error is dependent upon which apparatus are used in the measurement. The voltage - light and voltage - x-ray onset time delays involve error sources 1 through 6 above thus resulting in an overall error of ± 1.2 ns.

B. VOLTAGE MEASUREMENTS

Absolute signal strength was only important with the diode voltage signal because it was converted to actual diode voltage values using the method described in the experiment section of this paper. Since only relative signal strengths have any meaning for the light signals, no error analysis is necessary for the light signals. Sources of error for the diode voltage values determined in this experiment are shown in Table A.2 below.

Table B.2 VOLTAGE ERROR

Oscilloscope Vertical Plug-in 7B92A	$\pm 2\%$
Value of Attenuation	$\pm 5\%$
Digital interpretation by DCS w/zoom feature	$\pm 1\%$

These errors are are independent so they can also be added in quadrature resulting in an overall diode voltage error of 5.47% rounded up to 6%. However, when attempting to determine

the diode voltage at a certain instant in time, say at light or x-ray onset, the timing error must be taken into account. This was accomplished by estimating the slope of the voltage signal at the time of light onset, then estimating from this slope a voltage error based on the timing error involved. For the typical 55kv run the slope of the voltage signal was .05 V/ns with a ± 1.2 ns timing error this results in an oscilloscope voltage reading error of .06 V or with conversion to a diode voltage, we have a value of 19 kV. This must be added to a 6% error of the peak value of 1.83 V (± 0.11 V) oscilloscope error or a 35 kV diode voltage error. Summing the two we have a total error of ± 54 kV. The 75 kV shots have 3 V oscilloscope readings with slopes of about .2 V/ns. This results in a total error of 125 kV for the diode voltage at light onset. The 100 kV shots peak at 4 kV and have a slope of .4 V/ns, so the total diode voltage error is ± 230 kV.

LIST OF REFERENCES

1. "Onset of Breakdown in a Vacuum Diode", F. Schwirzke, X.K. Maruyama, S.A. Minnick, *Proceedings of the Eighth International Conference on High-Power Particle Beams, Vol.2*, World Scientific, Singapore, p. 958,1991.
2. Mesyats, G.A., and Proskurovsky, D.I., *Pulsed Electrical Discharge in Vacuum*, v.5, Springer-Verlag, 1989.
3. Hallal, M.P. Jr., *The Onset of Breakdown in a Fast Pulsed Vacuum Diode*, M.S. Thesis, Naval Postgraduate School, Monterey, California, June 1991.
4. Welsh, D.S., *Current Density Limitations in a Fast-Pulsed High-Voltage Diode*, M.S. Thesis, Naval Postgraduate School, Monterey, California, June 1992.
5. Schwirzke, F., *Laser Induced Breakdown and High Voltage Induced Vacuum Breakdown on Metal Surfaces*, *Laser Interaction and Related Plasma Phenomena, Vol 9*, pp. 335-357, H. Hora and G.H. Miley, eds., Plenum Publishing Corporation, 1991.
6. Miller, R.B., *An Introduction to the Physics of Intense Charged Particle Beams*, Plenum Press, 1982.
7. Schwirzke, F., Maruyama, X.K., and Hallal, M.P. Jr., *Ion Formation on the Surfaces of Electrodes*, *Nuclear Instruments and Methods in Physics Research*, Elsevier Science Publishers B.V., 1992.
8. Kittel, C., and Kroemer H., *Thermal Physics*, 2d ed., W.H. Freeman and Company, 1980.
9. Barnett, C.F., Ray, J.A., and Thompson, J.C., *Atomic and Molecular Collision Cross Sections of Interest in Controlled Thermonuclear Research*, p. 141, Oakridge National Laboratory, August 1964.
10. Wright, C., *Time Resolved Measurements of Light Produced By Onset of Plasma Formation on Electrodes of Fast Pulsed High Voltage Diodes*, Master's Thesis, Naval Postgraduate School, Monterey, California, December 1993.
11. Galarowicz, D., *Instrumentation Requirements for Tree Effects Data Collection at the Naval Postgraduate School Flash X-Ray Facility*, Master's Thesis, Naval Postgraduate School, Monterey, California, June 1990.

12. Physics International Company, *Model 112A Pulserad Pulsed X-Ray Generator Operations and Maintenance Manual*, January, 1986.
13. New Focus Inc., *Model 1601 Low Noise Photoreceiver User Manual*, 1992.
14. Fast Pulse Lasermetrics Inc., *Operator's Manual Series 3117, Type I*, 1984.
15. Tektronix Inc., *User Manual 7104 Oscilloscope*, 1986.
16. Tektronix Inc., *DCS01 Digitizing Camera System Software*, 1988.
17. Tektronix Inc., *User Manual DSA 602A*, 1992.
18. Hamamatsu Inc., *Silicon Photodiodes and Charge Sensitive Amplifiers for Scintillation Counting and High Energy Physics*, 1993.

INITIAL DISTRIBUTION LIST

	No. Copies
1. Defense Technical Information Center Cameron Station Alexandria VA 22304-6145	2
2. Library, Code 052 Naval Postgraduate School Monterey CA 93943-5002	2
3. Professor Fred Schwirzke, Code PH/Sw Department of Physics Naval Postgraduate School Monterey CA 93943-5000	2
4. Professor Xavier K. Maruyama, Code PH/Mx Department of Physics Naval Postgraduate School Monterey CA 93943-5000	2
5. Professor William B. Colson, Code PH/Cw Chairman, Department of Physics Naval Postgraduate School Monterey CA 93943-5000	1
6. Physics Library, Code PH Department of Physics Naval Postgraduate School Monterey CA 93943-5000	1
7. CPT Michael O. Callahan 1051 West Second Street Elmira NY 14905	2